1 **Trabecular and cortical bone structure of the talus and distal tibia in *Pan* and *Homo***

2 Zewdi J. Tsegai [1*], Matthew M. Skinner [2, 1], Andrew H. Gee [3], Dieter H. Pahr [4], Graham M. Treece [3],
3 Jean-Jacques Hublin [1], Tracy L. Kivell [2, 1]

4

5 Affiliations

6 [1] Department of Human Evolution, Max Planck Institute for Evolutionary Anthropology

7 [2] Skeletal Biology Research Centre, School of Anthropology and Conservation, University of Kent

8 [3] Department of Engineering, University of Cambridge

9 [4] Institute for Lightweight Design and Structural Biomechanics, Vienna University of Technology

10

11 * Corresponding author:

12 Zewdi Tsegai

13 Max Planck Institute for Evolutionary Anthropology

14 Department of Human Evolution

15 Deutscher Platz 6

16 D-04103 Leipzig

17 Germany

18

19

20 **Abbreviated title:** Internal bone structure of talus and tibia

21 **Keywords:** Bone microstructure, Functional morphology, Locomotion, Bipedalism, Cancellous bone

22 **Text pages:** 36; **Figures:** 10; **Tables:** 6

25

26

27

28

29

**ABSTRACT**

**Objectives:** Internal bone structure, both cortical and trabecular bone, remodels in response to loading and may provide important information regarding behaviour. The foot is well suited to analysis of internal bone structure because it experiences the initial substrate reaction forces, due to its proximity to the substrate. Moreover, as humans and apes differ in loading of the foot, this region is relevant to questions concerning arboreal locomotion and bipedality in the hominoid fossil record.

**Materials and methods:** We apply a whole-bone/epiphysis approach to analyse trabecular and cortical bone in the distal tibia and talus of *Pan troglodytes* and *Homo sapiens*. We quantify bone volume fraction (BV/TV), degree of anisotropy (DA), trabecular thickness (Tb.Th), bone surface to volume ratio (BS/BV), cortical thickness, and investigate the distribution of BV/TV and cortical thickness throughout the bone/epiphysis.

**Results:** We find that *Pan* has a greater BV/TV, a lower BS/BV and thicker cortices than *Homo* in both the talus and distal tibia. The trabecular structure of the talus is more divergent than the tibia, having thicker, less uniformly aligned trabeculae in *Pan* compared to *Homo*. Differences in dorsiflexion at the talocrural joint and in degree of mobility at the talonavicular joint are reflected in the distribution of cortical and trabecular bone.

**Discussion:** Overall, quantified trabecular parameters represent overall differences in bone strength between the two species, however, DA may be directly related to joint loading. Cortical and trabecular bone distributions correlate with habitual joint positions adopted by each species, and thus have potential for interpreting joint position in fossil hominoids.

54 **1. INTRODUCTION**

55 Aspects of the external bony morphology of the talus and distal tibia reflect kinematic differences

56 between how terrestrial bipedal humans and arboreal, quadrupedal African apes load their foot and ankle

57 during locomotion (e.g. Lewis, 1980a,b,c; Stern and Susman, 1983; Latimer et al., 1987; DeSilva, 2009;

58 Barak et al., 2013b). These morphological differences can be related to fundamental differences in foot

59 posture: the degree of dorsiflexion at the ankle, use of the foot in an inverted position, the general

60 conformation of the leg, and the presence of medial and longitudinal arches of the foot. For example,

61 compared with African apes, humans have been described as having a less mediolaterally expanded

62 anterior distal articular surface of the tibia (Latimer et al., 1987; DeSilva, 2009), an angle close to 90

63 degrees between the long axis and distal articular surface of the tibia (Latimer et al., 1987; DeSilva,

64 2009), a more symmetric talar trochlea (Latimer et al., 1987; DeSilva, 2009), a relatively stiff mid-foot

65 without a mid-tarsal break (Elftman and Manter, 1935; DeSilva, 2010), and a complex of features,

66 including the medial longitudinal arch, metatarsophalangeal joints and various soft tissues, which

67 contribute to the windlass mechanism (Griffin et al., 2015) that improves locomotor efficiency (Ker et al.,

68 1987).

69 In part due to the mosaic nature of fossil hominin morphology, but also due to reliance on fragmentary or

70 isolated postcranial elements, palaeoanthropologists often differ in their interpretations of the functional

71 significance of various morphological features. It remains unclear, based on the morphology of the ankle,

72 whether early hominins continued to engage in a significant amount of arboreal behaviour and whether

73 hominin species used kinematically similar or distinct forms of bipedalism, perhaps unlike the modern

74 human bipedal gait (e.g. Day and Wood, 1968; Lisowski et al., 1974; Lisowski et al., 1976; Oxnard and

75 Lisowski, 1980; Stern and Susman, 1983; Latimer et al., 1987; Clarke and Tobias, 1995; Harcourt-Smith

76 and Aiello, 2004; DeSilva, 2009; DeSilva and Throckmorton, 2010; Zipfel et al., 2011; Haile-Selassie et

77 al., 2012; DeSilva et al., 2013; Harcourt-Smith et al., 2015; Prang, 2015, 2016). Functional interpretation

78 of the external skeletal morphology of the foot is further complicated by the role of soft tissues in limiting

79    or enabling adoption of different foot postures (Venkataraman, 2013a,b) and by the substantial individual

80    variability in the flexibility of the modern human foot (Bates et al., 2013; DeSilva et al., 2015). As the

81    foot comprises a complex system of bones, tendons, ligaments and muscles, there are potentially many

82    different ways for it to adapt to different functions, other than by modification of external bone shape

83    (Crompton, 2015). Even modern humans are able to access numerous resources efficiently from the

84    arboreal environment (Kraft et al., 2014), without any apparent external morphological signal on the talus

85    and distal tibia (Venkataraman et al., 2013a).

86    Analysis of internal bone structure, both cortical and trabecular bone, of the talocrural and talonavicular

87    joint has potential to provide further insight into interpreting use of the foot in the past. While external

88    articular morphology indicates the joint positions a species was *able* to adopt, the internal bone structure

89    can provide information about how a joint was *actually* loaded (Ruff and Runestad, 1992; Kivell, 2016).

90    This is because both trabecular and cortical bone structure can adapt to loading during an individual's

91    lifetime (e.g. Lanyon, 1974; Robling et al., 2002; Pontzer et al., 2006; Ruff et al., 2006; Barak et al.,

92    2011; Kivell, 2016), by remodelling in response to strain (Ehrlich and Lanyon, 2002). Structural

93    adaptations can occur at the level of individual trabeculae (Schulte et al., 2013; Cresswell et al., 2015). As

94    these individual trabeculae appear able to adapt to accommodate regional strains, it is likely that regional

95    architectural parameters can provide information about how different areas of a joint are loaded. For

96    example, trabecular and cortical bone distribution close to the articular surface, radiodensity patterns, and

97    indicators of bone remodelling, correspond with predicted locations of peak loading associated with

98    specific joint positions (Patel and Carlson, 2007; Polk et al., 2008, 2010; Mazurier et al., 2010; Zeininger

99    et al., 2011; Carlson et al., 2013; Tsegai et al., 2013; Skinner et al., 2015).

100   Experimentally changing the loading regime of a joint or limb by, for example, changing the angle of the

101   joint during loading or subjecting a limb to an unnatural load, leads to predictable alterations in both

102   cortical and trabecular bone (Robling et al., 2002; Pontzer et al., 2006; Barak et al., 2011; Cresswell et al.,

103   2015). It is often difficult to relate bone structure, especially that of trabecular bone, directly to the

104    biomechanical environment, i.e. to connect specific architectural variables to joint function and loading

105    regime. Factors other than behaviour have the potential to influence, or even be the main factor

106    determining, bone form (Bertram and Swartz, 1991; Lovejoy et al., 2003; Ruff et al., 2006; Kivell, 2016).

107    There is still much that we do not fully understand about bone functional adaptation, including the genetic

108    and systemic factors that shape trabecular and cortical structure (Lieberman, 1996; Carlson et al., 2008;

109    Havill et al., 2010; Wallace et al., 2010; Paternoster et al., 2013; Wallace et al., 2013; Tsegai et al.,

110    2016a). These include the way in which bone remodels depending upon the duration, frequency, or

111    magnitude of the external load (e.g. Frost, 1987; Rubin and Lanyon, 1985; Skerry and Lanyon, 1995), or

112    how these factors might vary depending on species (e.g. Turner, 2001), anatomical region (e.g. Morgan

113    and Keaveny, 2001), age (e.g. Pearson and Lieberman, 2004) or body mass (e.g. Biewener, 1990; Doube

114    et al., 2011). Moreover, cortical and trabecular bone may respond differently to strain or even interact to

115    compensate for each other (Carlson and Judex, 2007). It is likely that these factors vary between even

116    closely related species/subspecies. For example, some of the genetic differences between modern humans

117    and Neanderthals relate to bone growth (Green et al., 2010), and changes in indirect measures of hormone

118    levels occur at different developmental stages in humans, chimpanzees and bonobos (e.g. TT3: Behringer

119    et al., 2014a; testosterone: Behringer et al., 2014b). All of these factors can confound our functional

120    interpretations of variation in bone structure. However, there is a wealth of comparative, computational

121    and *in vivo* research that makes clear that variation in cortical and trabecular structure reflects, at least to

122    some degree, variation in external loading (Ruff et al., 2006; Kivell, 2016).

123    The hominoid foot and ankle, specifically the talocrural and talonavicular joints, are well suited to

124    analysis of internal bone structure due to differences in foot postures adopted by modern humans and

125    extant apes, the specific structure of the joint, and the close association of the foot with the substrate.

126    Several studies have investigated the kinematics of the foot, during both quadrupedal and bipedal

127    locomotion, in humans and chimpanzees (e.g. Sockol et al., 2007; Pontzer et al., 2009; Pontzer et al.,

128    2014; O'Neill et al., 2015; Holowka et al., 2017). As modern human bipeds and chimpanzee

129 climbers/knuckle-walkers adopt divergent foot postures (DeSilva, 2009), the loading environment within

130 the foot and at the ankle is likely to differ between these groups. In *Pan troglodytes*, the ankle is loaded in

131 dorsiflexion during both vertical climbing and during quadrupedal knuckle-walking (Sockol et al., 2007;

132 DeSilva, 2009; Pontzer et al., 2009; Barak et al., 2013b; Pontzer et al., 2014), whereas the human ankle

133 adopts a more neutral posture during bipedalism (Barak et al., 2013b). The chimpanzee ankle is also

134 inverted during climbing (Lewis 1980a; Latimer et al., 1987; DeSilva, 2009). Loading at the talonavicular

135 joint is characterised by greater mobility in *Pan* compared to *Homo,* either related to dorsiflexion (i.e. the

136 midtarsal break) or to rotation (Elftman and Manter, 1935; DeSilva, 2010; Thompson et al., 2014; but see

137 Holowka et al., 2017). The high joint congruity between the distal tibia and the trochlea surface of the

138 talus (Latimer et al., 1987) indicates that the bone structure is likely to be directly related to joint use, and

139 not to other factors such as the action of muscles, as in other regions (e.g. the humeral head), where the

140 bony articulation itself does not maintain joint integrity. In the absence of muscle/tendon attachments on

141 the talus itself, and thus of tensile forces caused by muscle contractions, this region also offers an

142 opportunity to analyse the effects of locomotor forces alone on trabecular bone structure (DeSilva and

143 Devlin, 2012). Further, as the foot is in direct contact with the substrate, it directly experiences the initial

144 forces of locomotion, unlike more proximally located joints. The same is true for the hand, where clear

145 trabecular signals of the direction of loading are present (Tsegai et al., 2013; Skinner et al., 2015).

146 Previous analyses have assessed the functional significance of trabecular and cortical bone structure of the

147 ankle in humans (talus: Takechi et al., 1982; Sinha, 1985; Pal and Routal, 1998; Ebraheim et al., 1999;

148 Schiff et al., 2007; Athavale et al., 2008; Nowakowski et al., 2013; talus and distal tibia: Hvid et al.,

149 1985), and several studies have adopted a comparative approach across different taxa (talus: Su, 2011;

150 DeSilva and Devlin, 2012; Hérbert et al., 2012; Su et al., 2013; Su and Carlson, 2017; tibia: Su, 2011;

151 Barak et al., 2013b; Carlson et al., 2016). DeSilva and Devlin (2012) found interspecific differences in

152 regional patterning of trabecular structure across four quadrants of the talar body, but were unable to

153 attribute these differences to locomotor mode and a biomechanical explanation remains unclear. Analysis

154  of more localised subregions, sampling bone directly adjacent to the articular surface, has shown regional

155  patterning of degree of anisotropy (DA), elongation and primary trabecular orientation, which is distinct

156  in modern humans when compared with extant apes, with fossil hominins displaying some ape-like and

157  some human-like features (Su, 2011; Su et al., 2013; Su andCarlson, 2017). At the distal tibia, the

158  orientation of trabecular bone in humans and chimpanzees corresponds with measurements of

159  dorsiflexion at the ankle (Barak et al., 2013b). Previous studies have assessed cortical thickness and

160  radiodensity patterns of the articular surfaces of the primate talus and distal tibia (talus: Su, 2011; tibia:

161  Su, 2011; Carlson et al., 2016), and behavioural correlates have been identified from bone profiles and

162  radiodensity patterns at articular surfaces of other primate and mammalian taxa and epiphyses (Patel and

163  Carlson, 2007; Mazurier et al., 2010; Carlson et al., 2013). However, to our knowledge no previous study

164  has comparatively analysed cortical thickness maps in both the talus and distal tibia of humans and

165  chimpanzees.

166  Previous studies quantifying trabecular bone structure and/or bone strength characteristics at the ankle

167  relied on analyses of multiple volumes of interest (Su, 2011; DeSilva and Devlin, 2012; Su et al., 2013) or

168  on destructive methods (Sinha, 1985; Athavale et al., 2008). Interspecific analyses are often complicated

169  by the difficulty in identifying biologically homologous regions, and differences in VOI size and location

170  have a substantial impact on trabecular bone analysis, especially when comparing among species that

171  vary greatly in size and in morphologically complex bones (Maga et al., 2006; Kivell et al., 2011;

172  Lazenby et al., 2011). Moreover, trabecular bone close to the articular surface, which can be difficult to

173  sample using VOI-based methods that require manual discrimination between cortical and trabecular

174  bone, is more likely to be of biomechanical relevance as it experiences the initial joint reaction forces, and

175  bone closer to the articular surface differs from that in the center of the epiphysis (Singh, 1978). Analyses

176  of bone strength at the articular surface have not investigated the cortical and trabecular structure

177  independently, but have instead used methods which quantify cortical bone and some of the underlying

178  trabeculae (Patel and Carlson, 2007; Mazurier et al., 2010). In this study, we address some of these

179   challenges by using two methodologies that allow independent quantification of the trabecular and the

180   cortical structure. The trabecular bone analysis applied here enables quantification of trabecular structure

181   throughout the bone or in a pre-defined region of the epiphysis, however, statistical comparisons cannot

182   be conducted between groups. For cortical bone, we use a method that is able to compare cortical

183   thickness across the bone/epiphysis between groups, but does not allow quantification of trabecular

184   structure further than around 5mm beneath the cortex. By combining these complementary

185   methodologies, we are able to analyse patterns of both cortical and trabecular bone in the human and

186   chimpanzee talus and distal tibia. As a result, we are able to generate a fine scale, nuanced analysis

187   through the visualisation of regional patterning of both cortical and trabecular bone, which may provide

188   detailed information about joint loading.

189   In this study, we measure trabecular and cortical bone of the talus and distal tibia in *Pan troglodytes verus*

190   and *Homo sapiens*. We test the following predictions in how trabecular bone structure and distribution,

191   and cortical thickness and distribution differ between *Pan* and *Homo*. First, as both the talocrural and

192   talonavicular joint are used in a greater range of positions in *Pan*, and both joints are less mobile in

193   *Homo,* we predict a higher DA in humans in both the talus and tibia (Barak et al., 2013b; Su, 2011; Su et

194   al., 2013; Thompson et al., 2014; Su and Carlson, 2017; but see Holowka et al., 2017). Second, following

195   the findings of previous trabecular studies that sedentary modern humans have a generally low BV/TV

196   and cortical thickness (Ruff et al., 1993; Lieberman, 1996; Ruff, 2005; Chirchir et al., 2015; Ryan and

197   Shaw, 2015; Scherf et al., 2015; Chirchir et al., 2017), we predict an overall lower BV/TV and thinner

198   cortex in *Homo*. Third, we hypothesise that the regional distribution of both cortical and trabecular bone

199   will reflect differences in habitual peak loading of the talocrural and talonavicular joints. More

200   specifically, that at the talocrural joint *Pan* will show a pattern of BV/TV and cortical thickness that

201   reflects use of the foot in dorsiflexion and inversion, and at the talonavicular joint a greater degree of

202   mobility. In *Homo*, the trabecular bone distribution and cortical thickness will reflect less mobility, and a

203   more neutral ankle position.

204                                    **2. MATERIALS AND METHODS**

205                                             **2.1 Sample**

206    This study analysed trabecular and cortical bone morphology of the tibia and talus of two species with

207    divergent modes of locomotion: *Pan troglodytes verus* and *Homo sapiens*. The sample, detailed in Table

208    1, included fifteen wild *P. t. verus* individuals (tibiae: N = 10; tali: N = 13; of which N = 8 were paired)

209    whose skeletal remains were collected from the Taï National Park, Cote d'Ivoire, and ten *H. sapiens*

210    individuals (tibia: N = 8; tali: N = 9; of which N = 7 were paired) from an $18^{th}$ - $19^{th}$ century cemetery in

211    Inden, Germany. Adult specimens were used, based on fusion of the epiphyses throughout the skeleton

212    and no external signs of pathology or senescence related changes were present. The right side was chosen

213    where both talus and tibia were available and free from damage, otherwise the left side was used.


214                                    **2.2 Computed tomography**

215    High resolution micro-computed tomography (CT) scans were collected with a BIR ACTIS 225/300 CT

216    scanner for the tibiae and with a SkyScan1173 CT scanner for the tali, using an acceleration voltage of

217    130kV and 100μA and either a 0.5mm brass or 1mm aluminium filter, at the Department of Human

218    Evolution, Max Planck Institute for Evolutionary Anthropology (Leipzig, Germany). Isotropic acquisition

219    voxel sizes were 25-36 microns for the tibia and talus of *Homo* and 19-30 microns for the tibia and talus

220    of *Pan*. Each scan was reconstructed as a 2048 x 2048 16-bit TIFF image stack from 2500 projections

221    with three-frame averaging. Following reconstruction, all specimens were reoriented into standardised

222    positions using AVIZO 6.3® (Visualization Sciences Group, SAS) and segmented using a Ray Casting

223    Algorithm (Scherf and Tilgner, 2009).


224    Prior to segmentation, all *Pan* specimens were resampled to 35 microns and all *Homo* specimens to 40

225    microns, due to processing constraints. The relative resolutions, a measure of how adequately the average

226    trabecular strut is represented (i.e. mean trabecular thickness [mm] / resolution [mm]), are shown in Table

227    1. The average for the entire sample of 7.57 (range: 5.46 – 11.59) is consistent with previous studies of

228 trabecular bone structure (Sode et al., 2008; Kivell et al., 2011; Tsegai et al., 2013), and is appropriate for

229 microstructural analysis.

### 2.3 Analysis of trabecular bone microstructure

231 To quantify trabecular bone, each material in the scan (Fig. 1a), i.e. cortical bone, trabecular bone, air and

232 the internal bone cavity, were segmented automatically using an in house script in medtool v3.9 (www.dr-

233 pahr.at), following Gross et al. (2014). Morphological filters were used to separate these regions, and the

234 kernel size used was adjusted for each individual according to its measured trabecular thickness, enabling

235 an accurate, subject-specific segmentation. This resulted in three data sets that were used in subsequent

236 processing steps: (1) the trabecular bone (Fig. 1b), (2) the inner region of the bone and, (3) the inner mask

237 (Fig. 1c), which contains the internal region of the bone where internal bone cavity and trabecular bone

238 are represented by different grey values and the cortex has been removed. This automated segmentation

239 was problematic in two locations in the talus, at the inferior talar neck and at the subtalar joint surfaces,

240 due to their complex morphology. Thus the results from these regions are treated with caution. The

241 proximal boundary of the distal tibia was defined as the point at which curvature of the shaft begins in

242 both medial and anterior views, which is at the proximal extent of the fibular notch, and is an equivalent

243 location across the sample.

244 From the trabecular only mask (Fig. 1b), trabecular thickness (Tb.Th), bone surface area (BS), and bone

245 volume (BV) were quantified using the BoneJ plugin (version 1.3.12; Doube et al., 2010) for ImageJ

246 v1.46r (Schneider et al., 2012). Bone surface to volume ratio (BS/BV) was subsequently calculated.

247 The inner region of the bone was used to create a 3D tetrahedral mesh with a mesh size of 1mm, using

248 CGAL 4.4 (CGAL, Computational Geometry, http://www.cgal.org). The inner mask (Fig. 1c) was used to

249 calculate BV/TV throughout the bone to generate 3D colour maps of bone distribution, and to calculate

250 the overall bone volume fraction (BV/TV) and degree of anisotropy (DA) using medtool v3.9. A

251 rectangular background grid, with a grid size of 2.5mm, was applied and a spherical VOI with a diameter

252    of 5mm was used to measure BV/TV at each node of the grid. A sphere size of 5mm is appropriate as

253    enough trabecular struts are sampled to adequately quantify trabecular parameters (Gross et al., 2014). To

254    create a 3D colour map of bone distribution, the BV/TV values at each node were interpolated to assign

255    each element in the 3D mesh of the trabecular region a BV/TV value (Fig. 1d). The colour maps were

256    visualized in Paraview v4.0.1 (Ahrens et al., 2005). The overall BV/TV value was calculated as the mean

257    of the values for each element in the 3D mesh, and thus is the average for the whole bone/epiphysis. The

258    mean intercept method (Whitehouse, 1974; Odgaard, 1997) was used to calculate the mean fabric tensor,

259    the arithmetic mean of all second order fabric tensors normalised using the determinants. The extracted

260    eigenvalues and eigenvectors were then used to calculate the DA (DA = 1 − [smallest eigenvalue/largest

261    eigenvalue]), whereby a DA of 1 indicates complete anisotropy and a DA of 0 complete isotropy.

### 2.4 Analysis of cortical bone microstructure

263    To compare cortical thickness between *Pan* and *Homo* in the talus and distal tibia, cortical bone thickness

264    maps were generated for each specimen (following Treece et al., 2010; Treece et al., 2012; Tsegai et al.,

265    2016b). This was accomplished via semi-automatic segmentation of the cortical surface, from the

266    unsegmented CT data (Fig. 1e-f) in Stradwin v5.1a (Treece, Gee, Cambridge;

267    http://mi.eng.cam.ac.uk/~rwp/stradwin). Following definition of the surface, around 15,000 independent

268    measurements of cortical thickness were calculated throughout the bone (Fig. 1f) and mapped onto a

269    subject specific surface (Fig. 1g). Subsequently, each surface was registered to a canonical surface using

270    wxRegSurf v13 (Fig. 1h). The canonical surface used was an average of the entire sample, each species

271    was averaged separately and then the average of the two resulting surfaces was used, to prevent the

272    difference in sample size affecting the average morphology. After registration to the canonical surface,

273    mean thickness maps were generated for each species.

### 2.5 Statistical analysis

275    For trabecular bone analysis, all statistical tests were performed using R v3.0.3 (R Core Team, 2016) and

276    ggplot2 was used for generating plots (Wickham, 2009). Shapiro-Wilk test for normality showed that the

277    data were not normally distributed and thus non-parametric tests were used. Mann-Whitney U tests were

278    used to test for statistical differences in trabecular bone parameters between *Homo* and *Pan*. A principal

279    component analysis was conducted to determine which parameters contributed to interspecific differences

280    in the talus and in the tibia. All variables were included in the principal component analysis: Tb.Th,

281    BV/TV, DA, BS/BV, and cortical thickness. As there are large differences in the variances of these

282    variables, prior to analysis the data was centered and scaled to unit variance. Principal components were

283    subsequently derived by singular value decomposition of the resulting data matrix. Spearman's

284    correlation test and RMA regression were used to test for correlation between trabecular parameters and

285    cortical thickness in the talus and distal tibia. To test the relationship between size and trabecular bone

286    parameters, OLS $\log_{10}$ regressions and Pearson's correlation tests were conducted for each trabecular

287    parameter against the size of the epiphysis/bone for each taxon. The size of each bone was represented as

288    the geometric mean of several measurements, both of overall bone size and of the size of the articular

289    surfaces. For the talus, these measurements were the anteroposterior length, mediolateral width and

290    dorsoplantar height of the talus, the anteroposterior length and mediolateral width of the talar trochlea,

291    and the dorsoplantar height and mediolateral width of the talar head. For the tibia, a geometric mean was

292    derived from the maximum anteroposterior length and maximum mediolateral width of the distal tibia, the

293    anteroposterior length and mediolateral width of the distal articular surface, the anteroposterior length,

294    mediolateral width and proximodistal height of the medial malleolus. Pearson's correlation test was used

295    to compare trabecular parameters between paired tibia and tali in each taxon. Statistical parametric

296    mapping was used to identify regional cortical thickness differences between the two species (Friston et

297    al., 1995), using the SurfStat package (Worsley et al., 2009), by fitting a general linear model (GLM) to

298    the data. This model determined whether cortical thickness differences could be explained by species

299    (covariates of interest) or other factors (confounding covariates). As there is risk of systematic

300    misregistration due to shape differences, non-rigid shape coefficients were included as confounds in the

301    GLM (Gee and Treece, 2014; Gee et al., 2015). Bone size, however, was strongly correlated with species

302    and therefore not included as a confound in the GLM. Statistical parametric maps were generated using F

303    statistics and the corresponding p-values were corrected for multiple comparisons using random field

304    theory to control for the chance of false positives. Relative cortical thickness was calculated for each

305    specimen, by subtracting the individual mean value from each individual thickness measurement and

306    dividing by the standard deviation. In this way, relative patterns of cortical thickness could be analysed,

307    despite considerable interspecific differences in absolute cortical thickness. For all statistical tests, a *p*

308    value of <0.05 was considered significant.

## 3 RESULTS

### 3.1 Trabecular and cortical architecture of the talus and tibia

311    Means and standard deviations of measured trabecular and cortical parameters and Mann-Whitney U test

312    results are shown in Table 2, and extracted regions of trabecular bone, visualizing structural differences,

313    are shown in Figure 2. Mann-Whitney U test results (Table 2) find that the trabecular structure of *Pan*

314    differs from that of *Homo* in having a significantly greater BV/TV and lower BS/BV in both the talus and

315    the tibia. The trabecular structure is more divergent in the talus than in the tibia: with the talus of *Pan*

316    having significantly thicker, less uniformly-oriented trabeculae (i.e. lower DA). The cortex of *Pan* is

317    significantly thicker in both the talus and the tibia compared to *Homo*.

318    Correlations between parameters in the talus and tibia of each taxon are reported in Table 3. Significant

319    correlations between variables differ both between taxa and between skeletal regions. As such, all

320    parameters were included in the analysis, although correlations between parameters may lead to

321    overemphasis of the contribution of these variables. Table 4 shows the results of the principal component

322    (PC) analysis, and Figure 3 shows the plot of PC1 against PC2 for both the talus and tibia. Together, PC1

323    and PC2 explain 92.90% and 90.85% of the variance for the talus and tibia, respectively and in both

324    analyses, *Homo* and *Pan* are clearly separated. All four trabecular parameters and cortical thickness

325    contribute equally to PC1 in the talus, distinguishing *Pan*, with greater BV/TV, Tb.Th and cortical

326    thickness, but lower DA and BS/BV, from *Homo*. PC2 is driven by Tb.Th and BS/BV, but only separates

327    out particular individuals within each taxon. In the tibia, separation along PC1 is largely determined by

328  BV/TV, BS/BV and cortical thickness. Along PC2, most *Pan* individuals are distinguished from *Homo* in

329  having lower Tb.Th and higher DA.

## 3.2 Allometry

331  The results of the $\log_{10}$ OLS regressions of each parameter against the geometric mean, a proxy for bone

332  size, are shown for *Pan* and *Homo* in Table 5 and Figures 4 and 5. There were no significant correlations

333  between any trabecular parameter and bone size. However, the relationship between size and trabecular

334  and cortical structure does differ between species and between the talus and tibia (Figs. 4-5).

## 3.3 Correlation between the talus and tibia

336  Paired tali and tibiae were used to compare trabecular and cortical bone parameters between the talus and

337  tibia in seven *Homo* and eight *Pan* specimens (Table 6 and Fig. 6). Within *Pan*, all parameters other than

338  DA are strongly correlated across the joint (i.e. $r > 0.70$), whereas in *Homo*, only Tb.Th and BS/BV are

339  strongly and significantly correlated.

## 3.4 Distribution of trabecular bone in the talus and distal tibia

341  Figure 7 shows BV/TV colour maps for the talus of one representative individual of *Homo* and *Pan*.

342  Images of the full sample are included in the Supporting Information.

343  On the dorsal surface of the talus (Fig. 7 a and f), all *Pan* specimens share a region of high BV/TV on the

344  lateral edge of the trochlea. In some individuals this extends posteriorly along the edge, and in others it is

345  more anteriorly confined. Some, but not all, specimens have an additional region of higher BV/TV on the

346  medial trochlea, which is not consistent in its location or antero-posterior extent (see Supporting

347  Information). In *Homo*, there is no consistent pattern of trabecular bone distribution on the dorsal surface

348  of the trochlea as this region is highly variable across the sample. All individuals of both *Pan* and *Homo*

349  have a region of high BV/TV on the dorsal surface of the talar neck, although this is much more

350  pronounced in *Pan*. In a transverse plane, where the superior portion of the talus has been removed (Fig. 7

351  b and g), there is a region of high BV/TV at the neck in *Pan*, although, as mentioned above, the inferior

352  region of the neck must be interpreted with a certain degree of caution due to problems segmenting

353  trabeculae from cortex. In *Homo*, there is no localised region of high BV/TV in the neck, but instead an

354  anteroposterior trajectory of bone running through the head and neck, which is absent in *Pan*. The region

355  of high BV/TV at the articular surface of the talar head (i.e. at the talonavicular joint), is more localized in

356  *Homo* than in *Pan*. This is clearly seen in anterior view (Fig. 7 c and h), where *Homo* has a point of high

357  BV/TV located dorsally on the head, in contrast to *Pan*, where there is a band running mediolaterally

358  across the head. In the coronal (Fig. 7 d and i) and sagittal (Fig. 7 e and k) planes of *Homo,* the centre of

359  the talar body contains a relatively higher BV/TV than in *Pan.* Also, in the sagittal plane (Fig. 7 e and k)

360  there is a distinct trajectory of high BV/TV running antero-posteriorly through the talar head of *Homo* that

361  is not found in *Pan.* Instead, the *Pan* neck has a region of high BV/TV on the dorsal surface. Comparison

362  of the individual BV/TV scales shows that *Pan* has a higher BV/TV than *Homo* in both its minimum and

363  maximum values.

364  Colour maps of the BV/TV distribution in the distal tibia of *Homo* and *Pan* are shown in Figure 8 and

365  results for the entire sample are included in the Supporting Information. On the distal articular surface of

366  the tibia (Fig. 8a and e), some specimens of *Homo* have a high concentration of BV/TV confined to the

367  medial side of the articular surface and in other individuals it is centrally located. This is in contrast to

368  *Pan*, where there are consistently three regions of higher BV/TV: anterolateral, anteromedial and

369  posterocentral. When viewed in the mid-sagittal plane of the distal tibia (Fig. 8 b and f), the anteromedial

370  and posterior concentrations of bone are visible in *Pan,* in contrast to the more central and continuous

371  area of high BV/TV in *Homo*. On the anterior edge of the distal tibia (Fig. 8 c and g), *Pan* has a high

372  concentration of bone extending across the edge that is absent in *Homo*. In the mid-coronal plane (Fig. 8 d

373  and h), *Pan* contains a relatively greater BV/TV in the centre of the medial malleolus, compared to *Homo*.

374  Unlike the talus, the range of BV/TV is more similar between the two species (Fig 7 and Fig 8, scale

375  bars).

376                          **3.5 Distribution of cortical bone in the talus and distal tibia**

377    Mean relative cortical thickness maps for the talus and distal tibia of *Pan* and *Homo*, along with regions

378    of significant differences, are shown in Figures 9 and 10. In contrast to the trabecular bone maps, these

379    figures do not show the cortical thickness in just one individual, but rather the mean of all individuals by

380    taxon. As *Pan* has a greater cortical thickness in both the talus and the distal tibia, results are presented

381    for relative cortical thickness values, equalized by subtracting the mean value from each cortical thickness

382    value and dividing by the standard deviation for every individual in the sample.

383    Visual comparison between the relative cortical thickness maps of the talus in *Homo* (Fig. 9a) and *Pan*

384    (Fig. 9b), show that the regions of thickest cortical bone differ between the two species. On the talar head,

385    *Homo* has a dorsally located region of highest relative thickness, whereas in *Pan* the region of high

386    thickness runs mediolaterally along the dorsal half of the articular surface. At the trochlea, *Pan* has a

387    higher cortical thickness on the lateral edge, whereas in *Homo* it is the centromedial region that has the

388    highest mean thickness. *Pan* and *Homo* share thick cortical bone around the region of the talar neck,

389    however, in *Pan* this extends around the entire dorsal region of the neck, whereas in *Homo* it is confined

390    to the dorso-lateral side. In *Homo* the centre of the posterior subtalar articular surface has the thickest

391    cortical bone, whereas in *Pan* the cortical bone is thickest  anterolaterally on this articular surface.

392    Differences between *Pan* and *Homo* are shown in Figure 9c, and regions where these differences reach

393    significance are shown in Figure 9d. There are several regions with significant differences located at the

394    articular surfaces of the talus. *Pan* has relatively thinner bone compared to *Homo* on the anterior surface

395    of the talar head, on the anteromedial region of the talar trochlea and on the dorsal edge of the talar head,

396    and relatively thicker bone compared to *Homo* in a band anterolaterally on the posterior subtalar articular

397    surface.

398    Cortical thickness maps, showing relative cortical thickness are shown for *Homo* and *Pan* in Figure 10a

399    and b, respectively. In distal view, *Homo* has thickest cortical bone the along the medial edge of the distal

400    articular surface and the distal end of the medial malleolus. Both taxa share regions of thicker cortical

401    bone on the distal end of the medial malleolus and the medial edge of the distal articular surface. This

402  region on the medial articular surface is relatively thicker anteriorly in *Pan*, whereas in *Homo* this feature

403  extends along the medial border of the articular surface. *Pan* has two additional regions of thicker cortical

404  bone on the anterolateral and posterocentral regions of the distal articular surface. Comparisons of relative

405  cortical thickness values between *Homo* and *Pan* are shown in Figure 10c and regions with significant

406  differences are shown in Figure 10d. At the distal articular surfaces, *Pan* has significantly thicker cortex

407  at the anteromedial corner, extending along the anteromedial edge of the medial malleolus. There is

408  significantly thicker cortical bone on the distal surface of the medial malleolus in *Pan* compared to *Homo*.

409                                                     **4 DISCUSSION**

410  We analysed the internal bone structure of the talus and distal tibia in bipedal *Homo* and arboreal,

411  quadrupedal *Pan*. We find that trabecular and cortical bone, both the measured parameters and the

412  regional distribution of bone, differed, often significantly, between the two taxa in ways that are

413  potentially related to variation in joint position and load distribution during locomotion. In addition to

414  these differences, we find further support for previously proposed systemically weaker trabecular and

415  cortical bone in recent humans (Ruff et al., 1993; Lieberman, 1996; Ruff, 2005; Chirchir et al., 2015;

416  Ryan and Shaw, 2015; Scherf et al., 2015; Chichir et al., 2017).

417                          **4.1 Identifying functional signals in internal bone structure**

418  The relationship between bone form and mechanical loading is complex. It may be influenced by

419  numerous factors that affect bone growth and structure, which are likely to differ systematically between

420  species and, as such, bone structure should be considered within the broader context of what is already

421  known about the bone architecture of each species. In both the talus and distal tibia of *Homo*, we find

422  support for our prediction that bone is relatively weak, having a lower BV/TV, a higher BS/BV and

423  thinner cortices, compared with the more robust *Pan*. BV/TV is the strongest predictor of trabecular bone

424  stiffness, or Young's modulus; it alone explains 87-89% of variance in stiffness (Stauber et al., 2006;

425  Maquer et al., 2015). Cortical bone thickness is also related to bone strength, as thin cortices are

426  associated with increased fracture risk (Augat and Schorlemmer, 2006). The difference in trabecular

427    BV/TV and cortical thickness between *Pan* and *Homo* is consistent with previous findings for the talus

428    and distal tibia (talus: Su, 2011; DeSilva and Devlin, 2012; Su and Carlson, 2017; tibia: Su, 2011; Barak

429    et al., 2013b), and with the trabecular morphology of other anatomical regions (e.g. third metacarpal:

430    Tsegai et al., 2013; calcaneus: Maga et al., 2006; Zeininger et al., 2016; first and second metatarsal:

431    Griffin et al., 2010; systemic: Chirchir et al., 2015). As the biomechanical environment of different joints

432    in the human and chimpanzee are likely to vary given their divergent modes of locomotion, this consistent

433    difference across several anatomical sites may be part of a systemic pattern (i.e. in all regions of the

434    skeleton) and not due to specific locomotor, or other, behaviour. This gracility of the modern human

435    skeleton may be associated with increased sedentism following the adoption of agriculture, as early

436    hominins and recent hunter gatherers/foragers have a more robust skeleton (Ruff et al., 1993; Lieberman,

437    1996; Ruff, 2005; Chirchir et al., 2015; Ryan and Shaw, 2015; Scherf et al., 2015). Analysis of the

438    relationship between these structural parameters and size are limited by small sample sizes.

439    There are aspects of bone structure that appear likely to reflect joint function and thus can be of use for

440    reconstructing behaviour in the fossil record. Here, we find support for our prediction that the human talus

441    has a significantly higher DA than in *Pan*. However, contrary to our predictions, we find no significant

442    difference for the distal tibia. During human bipedalism the mid-foot forms a relatively rigid lever during

443    push off (Morris, 1977), compared with the flexibility of the chimpanzee mid-foot (Elftman and Manter,

444    1935; Susman, 1983; Thompson et al., 2014; but see Holowka et al., 2017). There is also less mobility at

445    the ankle of *Homo* than in *Pan* (Latimer et al., 1987). The less aligned trabeculae of the *Pan* talus are

446    consistent with being more able to withstand forces from multiple directions associated with a wider

447    range of joint positions, whereas the more highly aligned trabecular structure of the *Homo* talus appears to

448    reflect more stereotypical loading (Su, 2011; DeSilva and Devlin, 2012; Su et al., 2013; Su and Carlson,

449    2017). In contrast to previous studies (Su, 2011; Barak et al., 2013b), we do not find a higher DA in the

450    distal tibia of *Homo*, but rather higher (although not significantly so) mean DA in *Pan*.  However, Su

451    (2011) found that trabeculae in *Homo* were significantly more uniformly aligned in the talus compared

452     with the tibia, suggesting that more similar DA values in the *Homo* and *Pan* distal tibia are not

453     unexpected.

454     DA may hold a functional signal for different types of behaviour that engender more or less stereotypical

455     loads at a joint. Regional differences in DA have been useful in distinguishing between primate locomotor

456     groups, with the structure of the proximal femur being consistent with inferred differences in loading in

457     leaping and slow climbing strepsirrhines (Ryan and Ketcham, 2002a,b; MacLatchy and Muller, 2002;

458     Ketcham and Ryan, 2004). The trabecular structure of the human foot is generally more highly aligned

459     than other apes (first and second metatarsal: Griffin et al., 2010; calcaneus: Maga et al., 2006; Zeininger

460     et al., 2016; but see Kuo et al., 2013; talus: Su, 2011; Su et al., 2013; Su and Carlson, 2017). It seems

461     unlikely that this would relate to differences in activity level between the taxa,  and there are no consistent

462     differences in DA in the proximal femur (Ryan and Shaw, 2015) or humerus (Scherf et al., 2015) between

463     human populations with different activity levels (i.e. engaging in the same behaviours but at different

464     frequencies). Adult trabecular structure could reflect individual or interspecific differences in loading

465     during puberty, at a time when bone is more responsive to strain (e.g. Pettersson et al. 2010; for cortical

466     bone see Pearson and Lieberman, 2004). However, homologous regions of trabecular bone in adolescent

467     and adult humans have not been sampled, as many studies exploring ontogeny have investigated changes

468     in structure between non-adult groups (Ryan and Krovitz, 2006; Ryan et al., 2007; Gosman and Ketcham,

469     2009; Raichlen et al., 2015). DA in the proximal tibial metaphysis and in the ilium continue to change

470     between adolescence and adulthood (Gosman & Ketcham, 2009; Abel & Macho, 2011). Moreover,

471     chimpanzees reach adult-like locomotor behaviour by adolescence (Doran, 1992; Sarringhaus et al.,

472     2014), while humans reach this point during early childhood (e.g. Sutherland et al., 1980; Beck et al.,

473     1981; Raichlen et al., 2015). Trabecular orientation in the talus also shows plasticity later in life, as

474     degeneration of articular cartilage, i.e. changes at the joint surface that affect loading, is associated with

475     differences in trabecular orientation in humans (Schiff et al., 2007). This indicates that DA in adult

476     humans and chimpanzees is likely to reflect adult behaviour patterns, as loading from locomotion has

477 remained generally consistent during much of the later growth period. Together these results suggest that

478 the high degree of trabecular alignment throughout several elements of the human foot may be a

479 behavioural signal related to the stereotypical loading of terrestrial bipedality. We suggest that, using our

480 methodology, DA may provide functional information about loading in the talus, but not the tibia.

### 4.2 The relationship between joint position and bone distribution

482 We predicted that differences in the cortical and trabecular bone distribution maps would reflect variation

483 in dorsiflexion and inversion of the talocrural joint and the degree of mobility at the talonavicular joint.

484 The colour maps of cortical and trabecular bone support some, but not all, of these predictions. These

485 results are based on mean cortical thickness distribution maps and significant differences, and on BV/TV

486 distribution maps for each individual. Generation of mean morphometric maps for BV/TV was not

487 conducted due to the complexity of registering 3D meshes while ensuring homology.

### *4.2.1 Dorsiflexion*

489 Dorsiflexion at the ankle is characteristic of both climbing and knuckle-walking in chimpanzees

490 compared to the more neutral ankle posture adopted by humans during bipedalism. We find no clear

491 signal of dorsiflexion in trabecular and cortical bone of the talar trochlea, but are able to identify

492 differences in internal bone structure of the distal tibia that we propose are related to degree of

493 dorsiflexion. In chimpanzees, during knuckle-walking the angle between the long axis of the tibia and the

494 foot is 75.2 degrees, compared with 85.6 degrees in normal human bipedalism (Barak et al., 2013b).

495 During vertical climbing the degree of dorsiflexion is much greater, with an angle between the long axis

496 of the tibia and the foot of 44.5 degrees (DeSilva, 2009). The external morphology of the talar trochlea

497 and the distal articular surface of the tibia is associated with this difference in loading of the ankle

498 (DeSilva, 2009; but see Venkataraman et al., 2013a). It might be expected that the distribution of

499 trabecular bone and cortical bone in the talar trochlea of *Pan* would be more anteriorly distributed,

500 reflecting this difference in joint angle. However, we find no clear signal across the study sample in either

501 the trabecular or cortical bone distribution maps. This is consistent with previous studies that did not

502    identify differences in BV/TV across quadrants of the talar body (DeSilva and Devlin, 2012), or higher

503    BV/TV and cortical thickness in the anterior talar trochlea (Su, 2011; Su and Carlson, 2017).

504    In contrast to the talus, we did find that the trabecular and cortical bone structure of the distal tibia

505    reflected the differences in joint position between *Homo* and *Pan*. *Pan* shows two regions of higher

506    BV/TV and thicker cortical bone, located at the anterior portion of the distal articular surface of the tibia,

507    one lateral and one medial. In addition, the anterior edge of the distal articular surface has a higher

508    BV/TV, which extends up anteriorly through the epiphysis. This is in contrast to *Homo*, where BV/TV

509    maps show a more central concentration of trabecular bone. In *Homo,* the cortex is thickest on the medial

510    edge of the articular surface, adjacent to the medial malleolus. In several (but not all) individuals in the

511    study sample (see Supporting Information), this medial region also has a high BV/TV. Although direct

512    comparison between results from different subregions is complex, some of these findings are supported

513    by the results of Su (2011). Fewer significant differences in BV/TV and cortical thickness are found

514    across the *Homo* tibia compared to *Pan*, and *Pan* has generally higher BV/TV anteriorly and posteriorly.

515    This is not the case for cortical thickness, where both *Homo* and *Pan* have thicker bone on the antero- and

516    postero- medial regions, and in *Pan*, the posterocentral region of the articular surface (Su, 2011). Perhaps

517    also relevant to the degree of flexion at the ankle, there is a region of high BV/TV and cortical thickness

518    posterocentrally on the distal articular surface in *Pan*, with the region of high BV/TV extending into the

519    bone. This could indicate increased loading during plantarflexion in *Pan* compared to *Homo*, however,

520    this is not supported by kinematic data. Previous findings in the distal tibia of *Pan* also found that the

521    posterior region has a higher BV/TV than the central region, and thicker cortical bone was found in the

522    posterocentral region (Su, 2011; Su and Carlson, 2017).

523    In the absence of detailed kinematic data on joint contact areas, in particular for *Pan* (for humans see Wan

524    et al., 2006; Bae et al., 2015), our understanding of the differences in the loading of the trochlea in these

525    two species is limited. Moreover, we must make assumptions about which aspects of a species'

526    locomotor, or other, behaviour contribute most to the remodelling of bone. Previous studies in humans

527    have identified areas of contact and distribution of pressure on the talus using a finite element simulation

528    of the human foot during walking (Bae et al., 2015) and on both the talar trochlear and distal articular

529    surface of the tibia under pressure using dual orthogonal fluoroscopy (Wan et al., 2006; Caputo et al.,

530    2009; Bischof et al., 2010). During human bipedalism, ground reaction forces (GRF) peak at two phases,

531    first after heelstrike and before midstance, and second at toe off (Bae et al., 2015; Alexander, 2004), with

532    contact pressure and strain increasing throughout the stride, peaking at toe off (Bae et al., 2015). After

533    heelstrike, during the first peak in GRF, there is contact between the cartilage of the talus and tibia on the

534    latero-central trochlea (Wan et al., 2006; Bae et al., 2015). During stride, the area of contact moves

535    anteriorly (Wan et al., 2006; Bae et al., 2015) and the point of highest pressure moves anterocentrally

536    until toe off, when both the contact area and point of highest pressure are located on the anterior of the

537    trochlea, just lateral to the midline (Bae et al., 2015). At the distal tibia, contact is located antero-

538    posteriorly at heel strike, moving anteriorly across the medio-lateral extent of the articular surface at mid-

539    stance, and at heel strike in the anterolateral half of the distal articular surface of the tibia (Wan et al.,

540    2006). Although some of the human sample in this study have a region of high BV/TV on the anterior

541    talus, just lateral to the midline, near the location of highest pressure (Bae et al., 2015), this is not always

542    the region of highest BV/TV, and does vary within the sample. There is also no direct correspondence

543    between regions of contact and areas with thicker cortices. There are several potential explanations for

544    why the trabecular and cortical bone structure of the talar trochlea does not, as expected, reflect

545    differences in dorsiflexion at the ankle. Firstly, experimental measures of cartilage contact and pressure

546    may not necessarily correspond to the regions experiencing the greatest forces during life. Secondly,

547    modern humans differ greatly in their gait. For example, there is inter-individual variation in the presence

548    of a mid-tarsal break, and intra-individual variation between strides (Bates et al., 2013; DeSilva et al.,

549    2015). There is also variability in foot strike patterns, with individuals making initial contact with the

550    fore-foot, midfoot or heel, that could also contribute to variability in loading of the trochlea (e.g. during

551    running: Lieberman et al., 2010; Hatala et al., 2013). Thirdly, differences in the external morphology of

552    the talus may accommodate the different distribution of forces, i.e. different shaped tali absorb loads

553     differently, thus cortical thickness and trabecular architecture do not directly reflect differences in joint

554     position.

555     Due to interest in adaptations of the human skeleton to bipedal locomotion, many biomechanical analyses

556     of *Pan* have focused on bipedal walking (e.g. Susman, 1983; Thorpe et al., 2004; Wang et al., 2014;

557     O'Neill et al., 2015), although several studies have investigated kinematics of knuckle-walking in

558     bonobos (e.g. Vereecke et al., 2003; D'Août et al., 2004; Schoonaert et al., 2016). Although no *in vivo*

559     measurements of joint movement or cartilage contact are available for *Pan*, there is evidence of force

560     transmission due to contact between the anterior edge of the distal tibia and the neck of the talus. This can

561     be observed when manipulating dry, associated tibia and tali, where in an extreme position of dorsiflexion

562     the ankle joint retains congruity while there is contact between the talar neck and the anterior border of

563     the tibia in African apes, but not in *Homo* (Latimer et al., 1987). Modern humans who regularly adopt

564     crouched positions develop squatting faces on the talus and tibia (Boulle, 2001). The BV/TV distribution

565     may reflect this and indicate high loads transmitted through this region. On the medial and lateral side of

566     the talar neck and on the anteroinferior border of the tibia, *Pan* has regions of high BV/TV, which are

567     absent in *Homo*. This may reflect habitual loading of these regions in an ankle dorsiflexed to such a

568     degree that force transmission occurs between the antero-inferior edge of the distal tibia and the talar

569     neck.

570     *4.2.2 Talonavicular mobility*

571     We find a clear signal of differences in joint mobility at the talonavicular joint in the trabecular and

572     cortical bone structure. Two features in which human bipedalism is distinct from ape quadrupedalism are,

573     firstly, weight transfer from the lateral to medial side of the foot during midstance; and secondly, in

574     having a rigid mid-foot, so that the foot acts as a lever during toe off (Elftman and Manter, 1935). The

575     medial side of the midtarsal joint (the talonavicular joint) is more mobile than the lateral side

576     (calcaneocuboid and cuboid-MT5 joints), during stance phase the talus rotates, along with the leg and

577     calcaneus, creating a close packed talonavicular joint (Elftman, 1960; Siegler et al., 1988; Scott and

578     Winter, 1991). Although investigations of mid-foot mobility in *Pan* have largely focused on the mid-

579     tarsal break at the lateral side (DeSilva, 2010), there is greater movement at the talonavicular joint which,

580     during passive dorsiflexion of the foot, is characterised by rotation in the coronal plane (Thompson et al.,

581     2014). Furthermore, there is greater inter-individual and intra-individual variability in mobility of the

582     human lateral midfoot than was previously assumed (Elftman and Manter, 1935; Bates et al., 2013).

583     During bipedalism, humans have greater midfoot mobility during push off, which is characterised by

584     plantarflexion and adduction, whereas chimpanzees have higher dorsiflexion at the midfoot (mid-tarsal

585     break) during the single limb support period (Holowka et al., 2017). Contrary to expectations, the human

586     midfoot was found to be overall more mobile than that of chimpanzees (Holowka et al., 2017), however,

587     precise kinematics of the talonavicular joint remain unknown.

588     There are clear differences between the study taxa in the trabecular bone distribution at the talar head,

589     where *Pan* has a band of high BV/TV running mediolaterally across the talar head, and in *Homo* there is a

590     localised point of high BV/TV. In cortical thickness, *Pan* has relatively thinner cortices at the talar head,

591     which is significantly thinner in the central region. Previous studies have measured both trabecular bone

592     in the medial and lateral sides of the head (DeSilva and Devlin, 2012) and trabecular bone adjacent to the

593     neck of the talus (i.e. on the anteromedial region of the talar trochlea). When comparing the medial and

594     lateral side of the head of the talus in humans to other species, DeSilva and Devlin (2012) found no

595     significant difference in DA, although the trabeculae were significantly thicker in the lateral head and

596     significantly more connected in the medial head of humans compared to other species (DeSilva and

597     Devlin, 2012). In the anteromedial trochlea, humans have a unique orientation of trabeculae compared to

598     other great apes, in having trabeculae with a primarily anteroinferior orientation, i.e. parallel to the talar

599     neck; a pattern shared with an early Pleistocene biped, KNM-ER 1464 (Su, 2011; Su et al., 2013; Su and

600     Carlson, 2017). This distinct orientation of trabeculae in bipedal species noted by Su et al. (2013) may

601     correspond to the trajectory of bone that we show here, travelling through the talar head into the trochlea.

602   The trabecular and cortical distribution of the talar head reveals a clear difference in bone structure,

603   perhaps related to differences in midfoot mobility between the study species.

604   *4.2.3 Inversion*

605   As well as dorsiflexion, inversion of the foot is characteristic of arboreal behaviour in *Pan*, including

606   vertical climbing (DeSilva, 2009). Species that engage in more arboreal locomotion have a less

607   symmetrical trochlea surface, where the lateral trochlea ridge is higher than the medial. This asymmetry

608   increases the difference in the radius of curvature of the medial and lateral side, thereby increasing the

609   arcuate path of the tibia over the talus (Latimer et al., 1987), a difference that has even been identified

610   between more arboreal western and more terrestrial eastern gorillas (Dunn et al., 2014). Of potential

611   interest with regard to identifying signals of inversion, is the high BV/TV on the anterolateral lip of the

612   trochlea of the talus that is consistent throughout the sample of *Pan*. This region also has a slightly thicker

613   cortex in *Pan* than in *Homo*, with *Pan* having relatively thinner cortical bone than *Homo* on the

614   anteromedial region of the trochlea. This is consistent with previous findings of high BV/TV, but not

615   thicker cortices, on the anterolateral two thirds of the trochlea in *Pan* (Su, 2011; Su and Carlson, 2017).

616   This may reflect increased shearing stresses associated with adoption of inverted foot postures, which are

617   also mitigated by having a higher lateral ridge of the talus. More detailed understanding of the kinematics

618   of climbing and knuckle-walking, along with modelling of the forces experienced by the talus, may

619   improve interpretation of this signal.

620                                     **5 CONCLUSION**

621   Identifying those features of internal bone structure that are directly related to joint loading is often

622   problematic. Here, we find that average architectural variables (BV/TV, BS/BV and cortical thickness)

623   that relate to overall bone strength differ between *Pan* and *Homo*. These may be part of a systemic pattern

624   unrelated to joint function, but rather due to other factors such as overall activity levels, and therefore

625   may not be relevant for reconstructing loading of individual joints. However, the degree to which

626 trabeculae are uniformly oriented (DA) in the talus does correspond to variation in joint loading due to

627 different locomotor behaviours, clearly differentiating between the more stereotypical loading regime of

628 bipedalism in *Homo* and the greater range of motion and joint loading typical of arboreal behaviours in

629 *Pan*. In contrast to these architectural variables quantified throughout the epiphysis/bone, more precise

630 information about locomotor behaviour can be obtained from patterns of trabecular and cortical bone

631 distribution. The trabecular and cortical bone distribution of the distal tibia and talus reflect differences in

632 dorsiflexion at the ankle and range of motion at the talonavicular joint in humans and chimpanzees. Thus,

633 the distribution of both trabecular and cortical bone in the talus and distal tibia holds potential for

634 interpreting loading regimes and reconstructing loaded joint positions in fossil specimens.

642

643 **REFERENCES**

644 Abel, R., & Macho, G. A. (2011). Ontogenetic changes in the internal and external morphology of the
645 ilium in modern humans. *Journal of Anatomy*, 218, 324-335.

646 Ahrens, J., Geveci, B., & Law, C. (2005). ParaView: An end-user tool for large data visualization. In C.
647 D. Hansen & C. R. Johnson (Eds.), *Visualization Handbook* (pp. 717-731). Burlington: Butterworth-
648 Heinemann.

649 Alexander, R. M. (2004). Bipedal animals, and their differences from humans. *Journal of Anatomy*, 204,
650 321-330.

651 Athavale, S. A., Joshi, S. D., & Joshi S. S. (2008). Internal architecture of the talus. *Foot & Ankle*
652 *International*, 29, 82-86.

653  Augat, P., & Schorlemmer, S. (2006). The role of cortical bone and its microstructure in bone strength.
654  *Age and Ageing*, 35, 27-31.

655  Bae, J. Y., Park, K. S., Seon, J. K., & Jeon, I. (2015). Analysis of the effects of normal walking on ankle
656  joint contact characteristics after acute inversion ankle sprain. *Annals of Biomedical Engineering*, 43,
657  3015-3024.

658  Barak, M. M., Lieberman, D. E., & Hublin J.-J. (2013a). Of mice, rats and men: Trabecular bone
659  architecture in mammals scales to body mass with negative allometry. *Journal of Structural Biology*, 183,
660  123-131.

661  Barak, M. M., Lieberman, D. E., Raichlen, D., Pontzer, H., Warrener, A. G., & Hublin, J.-J. (2013b).
662  Trabecular evidence for a human-like gait in *Australopithecus africanus*. *PLoS ONE*, 8, e77687.

663  Barak, M. M., Lieberman, D. E., & Hublin, J.-J. (2011). A Wolff in sheep's clothing: Trabecular bone
664  adaptation in response to changes in joint loading orientation. *Bone*, 49, 1141-1151.

665  Bates, K. T., Collins, D., Savage, R., McClymont, J., Webster, E., Pataky, T. C., . . . Crompton, R. H.
666  (2013). The evolution of compliance in the human lateral mid-foot. *Proceedings of the Royal Society B:*
667  *Biological Sciences*, 280, 20131818.

668  Beck, R. J., Andriacchi, T. P., Kuo, K. N., Fermier, R. W., & Galante, J. O. (1981). Changes in the gait
669  patterns of growing children. *Journal of Bone and Joint Surgery*, 63A, 1452-1457.

670  Behringer, V., Deschner, T., Deimel, C., Stevens, J. M. G., & Hohmann, G. (2014a). Age-related changes
671  in urinary testosterone levels suggest differences in puberty onset and divergent life history strategies in
672  bonobos and chimpanzees. *Hormones and Behavior*, 66, 525–533.

673  Behringer, V., Deschner, T., Murtagh, R., Stevens, J. M. G., & Hohmann, G. (2014b). Age-related
674  changes in thyroid hormone levels of bonobos and chimpanzees indicate heterochrony in development.
675  *Journal of Human Evolution*, 66, 83-88.

676  Bertram, J. E. A., & Swartz, S. M. (1991). The 'law of bone transformation': A case of crying Wolff?
677  *Biological Reviews*, 66, 245-273.

678  Biewener, A. A. (1990). Biomechanics of mammalian terrestrial locomotion. *Science*, 250, 1097-1103.

679  Bischof, J. E., Spritzer, C. E., Caputo, A. M., Easley, M. E., DeOrio, J. K., Nunley, J. A., & DeFrate L. E.
680  (2010). In vivo cartilage contact strains in patients with lateral ankle instability. *Journal of Biomechanics*,
681  43, 2561-2566.

682  Boulle, E.-L. (2001). Evolution of two human skeletal markers of the squatting position: A diachronic
683  study from antiquity to the modern age. *American Journal of Physical Anthropology*, 115, 50-56.

684  Caputo, A. M., Lee, J. Y., Spritzer, C. E., Easley, M. E., DeOrio, J. K., Nunley, J. A., & DeFrate, L. E.
685  (2009). In vivo kinematics of the tibiotalar joint after lateral ankle instability. *The American Journal of*
686  *Sports Medicine*, 37, 2241-2248.

687  Carlson, K. J., Chirchir, H., & Patel, B. A. (2016). Subchondral properties of the hominoid distal tibia: An
688  indicator of loading during habitually dorsiflexed ankle postures. *American Journal of Physcial*
689  *Anthropology*, 159, 109.

690  Carlson, K. J., Jashashvili, T., Houghton, K., Westaway, M. C., & Patel, B. A. (2013). Joint loads in
691  marsupial ankles reflect habitual bipedalism versus quadrupedalism. *PLoS ONE*, 8, e58811.

692   Carlson, K. J., & Judex, S. (2007). Increased non-linear locomotion alters diaphyseal bone shape. *Journal*
693   *of Experimental Biology*, 210, 3117-3125.

694   Carlson, K. J., Lublinsky, S., & Judex, S. (2008). Do different locomotor modes during growth modulate
695   trabecular architecture in the murine hind limb? *Integrative and Comparative Biology*, 48, 385-393.

696   Chirchir, H., Kivell, T. L., Ruff, C. B., Hublin, J.-J., Carlson, K. J., Zipfel, B., & Richmond, B. G. (2015).
697   Recent origin of low trabecular bone density in modern humans. *Proceedings of the National Academy of*
698   *Sciences*, 112, 366-371.

699   Chirchir, H., Ruff, C. B., Junno, J.-A., & Potts, R. (2017). Low trabecular bone density in recent
700   sedentary modern humans. *American Journal of Physical Anthropology*, 162, 550-560.

701   Clarke, R. J., & Tobias, P. V. (1995). Sterkfontein Member 2 foot bones of the oldest South African
702   hominid. *Science*, 269, 521-524.

703   Cresswell, E. N., Goff, M. G., Nguyen, T. M., Lee, W. X., & Hernandez, C. J. (2015). Spatial
704   relationships between bone formation and mechanical stress within cancellous bone. *Journal of*
705   *Biomechanics*, 49, 222-228.

706   Crompton, R. H. (2015). The hominins: A very conservative tribe? Last common ancestors, plasticity and
707   ecomorphology in Hominidae. Or, what's in a name? *Journal of Anatomy*, 228, 686-699.

708   D'Août, K., Vereecke, E., Schoonaert, K., De Clercq, D., Van Elsacker, L., & Aerts, P. (2004).
709   Locomotion in bonobos (*Pan paniscus*): Differences and similarities between bipedal and quadrupedal
710   terrestrial walking, and a comparison with other locomotor modes. *Journal of Anatomy*, 204, 353-361.

711   Day, M. H., & Wood, B. A. (1968). Functional affinities of the Olduvai Hominid 8 talus. *Man*, 3, 440-
712   455.

713   DeSilva, J. M. (2009). Functional morphology of the ankle and the likelihood of climbing in early
714   hominins. *Proceedings of the National Academy of Sciences*, 106, 6567-6572.

715   DeSilva, J. M. (2010). Revisiting the "midtarsal break". *American Journal of Physical Anthropology*, 141,
716   245-258.

717   DeSilva, J. M., Bonne-Annee, R., Swanson, Z., Gill, C. M., Sobel, M., Uy, J., & Gill, S. V. (2015).
718   Midtarsal break variation in modern humans: Functional causes, skeletal correlates, and paleontological
719   implications. *American Journal of Physical Anthropology*, 156, 543-552.

720   DeSilva, J. M., & Devlin, M. J. (2012). A comparative study of the trabecular bony architecture of the
721   talus in humans, non-human primates, and *Australopithecus*. *Journal of Human Evolution*, 63, 536-551.

722   DeSilva, J. M., Holt, K. G., Churchill, S. E., Carlson, K. J., Walker, C. S., Zipfel, B., & Berger, L. R.
723   (2013). The lower limb and mechanics of walking in *Australopithecus sediba*. *Science,* 340, 1232999.

724   DeSilva, J. M., & Throckmorton, Z. J. (2010). Lucy's flat feet: The relationship between the ankle and
725   rearfoot arching in early hominins. *PLoS One*, 5, e14432.

726   Doran, D. M. (1992). The ontogeny of chimpanzee and pygmy chimpanzee locomotor behavior: A case
727   study of paedomorphism and its behavioral correlates. *Journal of Human Evolution*, 23, 139-157.

728 Doube, M., Kłosowski, M. M., Arganda-Carreras, I., Cordelières, F. P., Dougherty, R. P., Jackson, J. S., .
729 . . Shefelbine, S. J. (2010). BoneJ: Free and extensible bone image analysis in ImageJ. *Bone*, 47, 1076-
730 1079.

731 Doube, M., Klosowski, M. M., Wiktorowicz-Conroy, A. M., Hutchinson, J. R., & Shefelbine, S. J.
732 (2011).Trabecular bone scales allometrically in mammals and birds. *Proceedings of the Royal Society B:*
733 *Biological Sciences*, 278, 3067-3073.

734 Dunn, R. H., Tocheri, M. W., Orr, C. M., & Jungers, W. L. (2014). Ecological divergence and talar
735 morphology in gorillas. *American Journal of Physical Anthropology*, 153, 526-541.

736 Ebraheim, N. A., Sabry, F. F., & Nadim, Y. (1999). Internal architecture of the talus: Implication for talar
737 fracture. *Foot & Ankle International*, 20, 794-796.

738 Ehrlich, P. J., & Lanyon, L. E. (2002). Mechanical strain and bone cell function: A review. *Osteoporosis*
739 *International*, 13, 688-700.

740 Elftman, H. (1960). The transverse tarsal joint and its control. *Clinical Orthopaedics*, 16, 41-46.

741 Elftman, H., & Manter, J. (1935). Chimpanzee and human feet in bipedal walking. *American Journal of*
742 *Physical Anthropology*, 20, 69-79.

743 Friston, K. J., Holmes, A. P., Worsley, K. J., Poline, J.-P., Frith, C. D., & Frackowiak, R. S. J. (1995).
744 Statistical parametric maps in functional imaging: A general linear approach. *Human Brain Mapping*, 2,
745 189–210.

746 Frost, H. M. (1987). Bone "mass" and the "mechanostat": A proposal. *The Anatomical Record*, 219, 1-9.

747 Gee, A. H., & Treece, G. M. (2014). Systematic misregistration and the statistical analysis of surface data.
748 *Medical Image Analysis*, 18, 385-393.

749 Gee, A. H., Treece, G. M., Tonkin, C. J., Black D. M., & Poole, K. E. S. (2015). Association between
750 femur size and a focal defect of the superior femoral neck. *Bone*, 81, 60-66.

751 Gosman, J. H., & Ketcham, R. A. (2009). Patterns in ontogeny of human trabecular bone from SunWatch
752 Village in the Prehistoric Ohio Valley: General features of microarchitectural change. *American Journal*
753 *of Physical Anthropology*, 138, 318-332.

754 Green, R. E., Krause, J., Briggs, A. W., Maricic, T., Stenzel, U., Kircher, M., … Pääbo, S. (2010). A draft
755 sequence of the Neandertal genome. *Science*, 328, 710-722.

756 Griffin, N. L., D'Août, K., Ryan, T. M., Richmond, B. G., Ketcham, R. A., & Postnov, A. (2010).
757 Comparative forefoot trabecular bone architecture in extant hominids. *Journal of Human Evolution*, 59,
758 202-213.

759 Griffin, N. L., Miller, C. E., Schmitt, D., & D'Août, K. (2015). Understanding the evolution of the
760 windlass mechanism of the human foot from comparative anatomy: Insights, obstacles, and future
761 directions. *American Journal of Physical Anthropology*, 156, 1-10.

762 Gross, T., Kivell, T. L., Skinner, M. M., Nguyen, N. H., & Pahr, D. H. (2014). A CT-image-based
763 framework for the holistic analysis of cortical and trabecular bone morphology. *Palaeontologia*
764 *Electronica*, 17, 33A.

765 Haile-Selassie, Y., Saylor, B. Z., Deino, A., Levin, N. E., Alene, M., & Latimer, B. M. (2012). A new
766 hominin foot from Ethiopia shows multiple Pliocene bipedal adaptations. *Nature*, 483, 565-570.

767 Harcourt-Smith, W. E. H., & Aiello, L. C. (2004). Fossils, feet and the evolution of human bipedal
768 locomotion. *Journal of Anatomy*, 204, 403-416.

769 Harcourt-Smith, W. E. H., Throckmorton, Z., Congdon, K. A., Zipfel, B., Deane, A. S., Drapeau, M. S.
770 M., . . . DeSilva, J. M. (2015). The foot of *Homo naledi*. *Nature Communications*, 6, 8432.

771 Hatala, K. G., Dingwall, H. L., Wunderlich, R. E., & Richmond, B. G. (2013). Variation in foot strike
772 patterns during running among habitually barefoot populations. *PLoS One, 8*(1), e52548.

773 Havill, L. M., Allen, M. R., Bredbenner, T. L., Burr, D. B., Nicolella, D. P., Turner, C. H., . . . Mahaney,
774 M. C. (2010). Heritability of lumbar trabecular bone mechanical properties in baboons. *Bone*, 46, 835-
775 840.

776 Hérbert, D., Lebrun, R., & Marivaux, L. (2012). Comparative three-dimensional structure of the
777 trabecular bone in the talus of primates and its relationship to ankle joint loads generated during
778 locomotion. *The Anatomical Record*, 295, 2069-2088.

779 Holowka, N. B., O'Neill, M. C., Thompson, N. E., & Demes, B. (2017). Chimpanzee and human midfoot
780 motion during bipedal walking and the evolution of the longitudinal arch of the foot. *Journal of Human
781 Evolution*, 104, 23-31.

782 Hvid, I., Rasmussen, O., Jensen, N. C., & Nielsen, S. (1985). Trabecular bone strength profiles at the
783 ankle joint. *Clinical Orthopaedics and Related Research*, 199, 306-312.

784 Ker, R. F., Bennett, M. B., Bibby, S. R., Kester, R. C., & Alexander, R. M. (1987). The spring in the arch
785 of the human foot. *Nature*, 325, 147-149.

786 Ketcham, R. A., & Ryan, T. M. (2004). Quantification and visualization of anisotropy in trabecular bone.
787 *Journal of Microscopy*, 213, 158-171.

788 Kivell, T. L. (2016). A review of trabecular bone functional adaptation: What have we learned from
789 trabecular analyses in extant hominoids and what can we apply to fossils? *Journal of Anatomy*, 228, 569-
790 594.

791 Kivell, T. L., Skinner, M. M., Lazenby, R., & Hublin, J.-J. (2011). Methodological considerations for
792 analyzing trabecular architecture: An example from the primate hand. *Journal of Anatomy*, 218, 209-225.

793 Kraft, T. S., Venkataraman, V. V., & Dominy, N. J. (2014). A natural history of human tree climbing.
794 *Journal of Human Evolution*, 71, 105-118.

795 Kuo, S., DeSilva, J. M., Devlin, M. J., McDonald, G., & Morgan, E. F. (2013). The effect of the Achilles
796 tendon on trabecular structure in the primate calcaneus. *The Anatomical Record*, 296, 1509-1517.

797 Lanyon, L. E. (1974). Experimental support for the trajectorial theory of bone structure. *The Journal of
798 Bone and Joint Surgery*, 56, 160-166.

799 Latimer, B., Ohman, J. C., & Lovejoy, C. O. (1987). Talocrural joint in African hominoids: Implications
800 for *Australopithecus afarensis*. *American Journal of Physical Anthropology*, 74, 155-175.

801 Lazenby, R. A., Skinner, M. M., Kivell, T. L., & Hublin, J.-J. (2011). Scaling VOI size in 3D μCT studies
802 of trabecular bone: A test of the over-sampling hypothesis. *American Journal of Physical Anthropology*,
803 144, 196-203.

804 Lewis, O. J. (1980a). The joints of the evolving foot. Part I. The ankle joint. *Journal of Anatomy*, 130,
805 527-543.

806 Lewis, O. J. (1980b). The joints of the evolving foot. Part II. The intrinsic joints. *Journal of Anatomy*,
807 130, 833-857.

808 Lewis, O. J. (1980c). The joints of the evolving foot. Part III. The fossil evidence. *Journal of Anatomy*,
809 131, 275-298.

810 Lieberman, D. E. (1996). How and why humans grow thin skulls: Experimental evidence for systemic
811 cortical robusticity. *American Journal of Physical Anthropology*, 101, 217-236.

812 Lieberman, D. E., Venkadesan, M., Werbel, W. A., Daoud, A. I., D'Andrea, S., Davis, I. S., . . . Pitsiladis,
813 Y. (2010). Foot strike patterns and collision forces in habitually barefoot versus shod runners. *Nature*,
814 463(7280), 531-535.

815 Lisowski, F. P., Albrecht, G. H., & Oxnard, C. E. (1974). The form of the talus in some higher primates:
816 A multivariate study. *American Journal of Physical Anthropology*, 41, 191-216.

817 Lisowski, F. P., Albrecht, G. H., & Oxnard, C. E. (1976). African fossil tali: Further multivariate
818 morphometric studies. *American Journal of Physical Anthropology*, 45, 5-18.

819 Lovejoy, C. O., McCollum, M. A., Reno, P. L., & Rosenman, B. A. (2003). Developmental biology and
820 human evolution. *Annual Review of Anthropology*, 32, 85-109.

821 MacLatchy, L., & Müller, R. (2002). A comparison of the femoral head and neck trabecular architecture
822 of *Galago* and *Perodicticus* using micro-computed tomography (μCT). *Journal of Human Evolution*, 43,
823 89-105.

824 Maga, M., Kappelman, J., Ryan, T. M., & Ketcham, R. A. (2006). Preliminary observations on the
825 calcaneal trabecular microarchitecture of extant large-bodied hominoids. *American Journal of Physical
826 Anthropology*, 129, 410-417.

827 Maquer, G., Musy, S. N., Wandel, J., Gross, T., & Zysset, P. K. (2015). Bone volume fraction and fabric
828 anisotropy are better determinants of trabecular bone stiffness than other morphological variables.
829 *Journal of Bone and Mineral Research*, 30, 1000-1008.

830 Mazurier, A., Nakatsukasa, M., & Macchiarelli, R. (2010). The inner structural variation of the primate
831 tibial plateau characterized by high-resolution microtomography. Implications for the reconstruction of
832 fossil locomotor behaviours. *Comptes Rendus Palevol*, 9, 349-359.

833 Morgan, E. F., & Keaveny, T. M. (2001). Dependence of yield strain of human trabecular bone on
834 anatomic site. *Journal of Biomechanics*, 34, 569-577.

835 Morris, J. M. (1977). Biomechanics of the foot and ankle. *Clinical Orthopaedics and Related Research*,
836 122, 10-17.

837 Nowakowski, A. M., Deyhle, H., Zander, S., Leumann, A., & Müller-Gerbl, M. (2013). Micro CT
838 analysis of the subarticular bone structure in the area of the talar trochlea. *Surgical and Radiologic
839 Anatomy*, 35, 283-293.

840  Odgaard, A. (1997). Three-dimensional methods for quantification of cancellous bone architecture. *Bone*,
841  20, 315-328.

842  O'Neill, M. C., Lee, L.-F., Demes, B., Thompson, N. E., Larson, S. G., Stern Jr, J. T., & Umberger, B. R.
843  (2015). Three-dimensional kinematics of the pelvis and hind limbs in chimpanzee (*Pan troglodytes*) and
844  human bipedal walking. *Journal of Human Evolution*, 86, 32-42.

845  Oxnard, C. E., & Lisowski, F. P. (1980). Functional articulation of some hominoid foot bones:

846  Implications for the Olduvai (Hominid 8) foot. *American Journal of Physical Anthropology*, 52, 107-117.

847  Pal, G. P., & Routal, R. V. (1998). Architecture of the cancellous bone of the human talus. *The
848  Anatomical Record*, 252, 185-193.

849  Patel, B. A., & Carlson, K. J. (2007). Bone density spatial patterns in the distal radius reflect habitual
850  hand postures adopted by quadrupedal primates. *Journal of Human Evolution*, 52, 130-141.

851  Paternoster, L., Lorentzon, M., Lehtimäki, T., Eriksson, J., Kähönen, M., Raitakari, O., . . . Ohlsson, C.
852  (2013). Genetic determinants of trabecular and cortical volumetric bone mineral densities and bone
853  microstructure. *PLoS Genetics*, 9, e1003247.

854  Pearson, O. M., & Lieberman, D. E. (2004). The aging of Wolff's 'law': Ontogeny and responses to
855  mechanical loading in cortical bone. *Yearbook of Physical Anthropology*, 47, 63-99.

856  Pettersson, U., Nilsson, M., Sundh, V., Mellström, D., & Lorentzon, M. (2010). Physical activity is the
857  strongest predictor of calcaneal peak bone mass in young Swedish men. *Osteoporosis International*, 21,
858  447-455.

859  Polk, J. D., Blumenfeld, J., & Ahluwalia, D. (2008). Knee posture predicted from subchondral apparent
860  density in the distal femur: An experimental validation. *The Anatomical Record*, 291, 293-302.

861  Polk, J. D., Williams, S. A., Peterson, J. V., Roseman, C. C., & Godfrey, L. R. (2010). Subchondral bone
862  apparent density and locomotor behavior in extant primates and subfossil lemurs Hadropithecus and
863  Pachylemur. International Journal of Primatology, 31, 275-299.

864  Pontzer, H., Lieberman, D. E., Momin, E., Devlin, M. J., Polk, J. D., Hallgrímsson, B., & Cooper, D. M.
865  L. (2006). Trabecular bone in the bird knee responds with high sensitivity to changes in load orientation.
866  *The Journal of Experimental Biology*, 209, 57-65.

867  Pontzer, H., Raichlen, D. A., & Rodman, P. S. (2014). Bipedal and quadrupedal locomotion in
868  chimpanzees. *Journal of Human Evolution*, 66, 64-82.

869  Pontzer, H., Raichlen, D. A., & Sockol, M. D. (2009). The metabolic cost of walking in humans,
870  chimpanzees, and early hominins. *Journal of Human Evolution*, 56, 43-54.

871  Prang, T. C. (2015). Rearfoot posture of *Australopithecus sediba* and the evolution of the hominin
872  longitudinal arch. *Scientific Reports*, 5, 17677.

873  Prang, T. C. (2016). The subtalar joint complex of *Australopithecus sediba*. *Journal of Human Evolution*,
874  90, 105-119.

875  Raichlen, D. A., Gordon, A. D., Foster, A. D., Webber, J. T., Sukhdeo, S. M., Scott, R. S., . . . Ryan, T.
876  M. (2015). An ontogenetic framework linking locomotion and trabecular bone architecture with
877  applications for reconstructing hominin life history. *Journal of Human Evolution*, 81, 1-12.

878    R Core Team. (2016). R: A language and environment for statistical computing. R Foundation for
879    Statistical Computing, Vienna, Austria. URL https://www.R-project.org/

880    Robling, A. G., Hinant, F. M., Burr, D. B., & Turner, C. H. (2002). Improved bone structure and strength
881    after long-term mechanical loading is greatest if loading is separated into short bouts. *Journal of Bone*
882    *and Mineral Research*, 17, 1545-1554.

883    Rubin, C. T., & Lanyon, L. E. (1985). Regulation of bone mass by mechanical strain magnitude. *Calcified*
884    *Tissue International*, 37, 411-417.

885    Ruff, C. B. (2005). Mechanical determinants of bone form: Insights from skeletal remains. *Journal of*
886    *Musculoskeletal Neuronal Interactions*, 5, 202-212.

887    Ruff, C., Holt, B., & Trinkaus, E. (2006). Who's afraid of the big bad Wolff? "Wolff's law" and bone
888    functional adaptation. *American Journal of Physical Anthropology*, 129, 484-498.

889    Ruff, C. B., & Runestad, J. A. (1992). Primate limb bone structural adaptations. *Annual Review of*
890    *Anthropology*, 21, 407-433.

891    Ruff, C. B., Trinkaus, E., Walker, A., & Larsen, C. S. (1993). Postcranial robusticity in *Homo*, I:
892    Temporal trends and mechanical interpretation. *American Journal of Physical Anthropology*, 91, 21-53.

893    Ryan, T. M., & Ketcham, R. A. (2002a). The three-dimensional structure of trabecular bone in the
894    femoral head of strepsirrhine primates. *Journal of Human Evolution*, 43, 1-26.

895    Ryan, T. M., & Ketcham, R. A. (2002b). Femoral head trabecular bone structure in two omomyid
896    primates. *Journal of Human Evolution*, 43, 241-263.

897    Ryan, T. M., & Krovitz, G. E. (2006). Trabecular bone ontogeny in the human proximal femur. *Journal*
898    *of Human Evolution*, 51, 591-602.

899    Ryan, T. M., & Shaw, C. N. (2015). Gracility of the modern *Homo sapiens* skeleton is the result of
900    decreased biomechanical loading. *Proceedings of the National Academy of Sciences*, 112, 372-377.

901    Ryan, T. M., van Rietbergen, B., & Krovitz, G. (2007). Mechanical adaptation of the trabecular bone in
902    the growing human femur and humerus. *American Journal of Physical Anthropology*, 44, 203.

903    Sarringhaus, L. A., MacLatchy, L. M., & Mitani, J. C. (2014). Locomotor and postural development of
904    wild chimpanzees. *Journal of Human Evolution*, 66, 29-38.

905    Scherf, H., & Tilgner, R. (2009). A new high-resolution computed tomography (CT) segmentation
906    method for trabecular bone architectural analysis. *American Journal of Physical Anthropology*, 140, 39-
907    51.

908    Scherf, H., Wahl, J., Hublin, J.-J., & Harvati, K. (2015). Patterns of activity adaptation in humeral
909    trabecular bone in Neolithic humans and present-day people. *American Journal of Physical Anthropology*,
910    159, 106-115.

911    Schiff, A., Li, J., Inoue, N., Masuda, K., Lidtke, R., & Muehleman, C. (2007). Trabecular angle of the
912    human talus is associated with the level of cartilage degeneration. *Journal of Musculoskeletal and*
913    *Neuronal Interactions*, 7, 224-230.

914    Schneider, C. A., Rasband, W. S., & Eliceiri, K. W. (2012). NIH Image to ImageJ: 25 years of image
915    analysis. *Nature Methods*, 9, 671-675.

916  Schoonaert, K., D'Août, K., Samuel, D., Talloen, W., Nauwelaerts, S., Kivell, T. L., & Aerts, P. (2016).
917  Gait characteristics and spatio-temporal variables of climbing in bonobos (*Pan paniscus*). *American*
918  *Journal of Primatology*, 78, 1165-1177.

919  Schulte, F. A., Ruffoni, D., Lambers, F. M., Christen, D., Webster, D. J., Kuhn, G., & Müller, R. (2013).
920  Local mechanical stimuli regulate bone formation and resorption in mice at the tissue level. *PLoS ONE*, 8,
921  e62172.

922  Scott, S. H., & Winter, D. A. (1991). Talocrural and talocalcaneal joint kinematics and kinetics during the
923  stance phase of walking. *Journal of Biomechanics*, 24, 743-752.

924  Siegler, S., Chen, J., & Schneck, C. D. (1988). The three-dimensional kinematics and flexibility
925  characteristics of the human ankle and subtalar joints: Part I: Kinematics. *Journal of Biomechanical*
926  *Engineering*, 110, 364-373.

927  Singh, I. (1978). The architecture of cancellous bone. *Journal of Anatomy*, 127, 305-310.

928  Sinha, D. N. (1985). Cancellous structure of tarsal bones. *Journal of Anatomy*, 140, 111-117.

929  Smith, R. J., & Jungers, W. L. (1997). Body mass in comparative primatology. *Journal of Human*
930  *Evolution*, 32, 523-559.

931  Skerry, T. M., & Lanyon, L. E. (1995). Interruption of disuse by short duration walking exercise does not
932  prevent bone loss in the sheep calcaneus. *Bone*, 16, 269-274.

933  Skinner, M. M., Stephens, N. B., Tsegai, Z. J., Foote, A. C., Nguyen, N. H., Gross, T., Pahr, D. H.,
934  Hublin, J.-J., & Kivell, T. L. (2015). Human-like hand use in *Australopithecus africanus*. *Science*, 347,
935  395-399.

936  Sode, M., Burghardt, A. J., Nissenson, R. A., & Majumdar, S. (2008). Resolution dependence of the non-
937  metric trabecular structure indices. *Bone*, 42, 728-736.

938  Sockol, M. D., Raichlen, D. A., & Pontzer, H. (2007). Chimpanzee locomotor energetics and the origin of
939  human bipedalism. *Proceedings of the National Academy of Sciences*, 104(30), 12265-12269.

940  Stauber, M., Rapillard, L., van Lenthe, G. H., Zysset, P., & Müller, R. (2006). Importance of individual
941  rods and plates in the assessment of bone quality and their contribution to bone stiffness. *Journal of Bone*
942  *and Mineral Research*, 21, 586-595.

943  Stern, J. T., & Susman, R. L. (1983). The locomotor anatomy of *Australopithecus afarensis*. *American*
944  *Journal of Physical Anthropology*, 60, 279-317.

945  Su, A. (2011). *The Functional Morphology of Subchondral and Trabecular Bone in the Hominoid*
946  *Tibiotalar Joint*. (Doctoral dissertation, Stony Brook University).  Retrieved from
947  https://dspace.sunyconnect.suny.edu/handle/1951/56131

948  Su, A., & Carlson, K. J. (2017). Comparative analysis of trabecular bone structure and orientation in
949  South African hominin tali. *Journal of Human Evolution*, 106, 1-18.

950  Su, A., Wallace, I. J., & Nakatsukasa, M. (2013). Trabecular bone anisotropy and orientation in an Early
951  Pleistocene hominin talus from East Turkana, Kenya. *Journal of Human Evolution*, 64, 667-677.

952  Susman, R. L. (1983). Evolution of the human foot: Evidence from Plio-Pleistocene hominids. *Foot &*
953  *Ankle*, 3, 365-376.

954 Sutherland, D. H., Olshen, R., Cooper, L., & Woo, S. L. Y. (1980). The development of mature gait.
955 *Journal of Bone and Joint Surg*ery, 62A, 336-353.

956 Takechi, H., Ito, S., Takada, T., & Nakayama, H. (1982). Trabecular architecture of the ankle joint.
957 *Anatomia Clinica*, 4, 227-233.

958 Thompson, N. E., Holowka, N. B., O'Neill, M. C., & Larson, S. G. (2014). Brief communication:
959 Cineradiographic analysis of the chimpanzee (*Pan troglodytes*) talonavicular and calcaneocuboid joints.
960 *American Journal of Physical Anthropology*, 154, 604-608.

961 Thorpe, S. K. S., Crompton, R. H., & Wang, W. J. (2004). Stresses exerted in the hindlimb muscles of
962 common chimpanzees (*Pan troglodytes*) during bipedal locomotion. *Folia Primatologica*, 75, 253-265.

963 Treece, G. M., Gee, A. H., Mayhew, P. M., & Poole, K. E. S. (2010). High resolution cortical bone
964 thickness measurement from clinical CT data. *Medical Image Analysis*, 14, 276-290.

965 Treece, G. M., Poole, K. E. S., & Gee, A. H. (2012). Imaging the femoral cortex: Thickness, density and
966 mass from clinical CT. *Medical Image Analysis*, 16, 952-965.

967 Tsegai, Z. J., Kivell, T. L., Gross, T., Nguyen, N. H., Pahr, D. H., Smaers, J. B., & Skinner, M. M.
968 (2013). Trabecular bone structure correlates with hand posture and use in hominoids. *PLoS One*, 8,
969 e78781.

970 Tsegai, Z. J., Skinner, M. M., Pahr, D. H., Hublin, J.-J., & Kivell, T. L. (2016a). Systemic patterns of
971 trabecular structure in *Homo* and *Pan*: Evaluating inter- and intraspecific variability across anatomical
972 sites. *American Journal of Physical Anthropology*, 159, 318.

973 Tsegai, Z. J., Stephens, N. S., Treece, G., Skinner, M. M., Kivell, K. L., & Gee, A. (2016b). Cortical bone
974 mapping: An application to hand and foot bones in hominoids. *Comptes Rendus Palevol*,
975 http://doi.org/10.1016/j.crpv.2016.11.001

976 Turner, A. S. (2001). Animal models of osteoporosis – necessity and limitations. *European Cells and*
977 *Materials*, 1, 66-81.

978 Venkataraman, V. V., Kraft, T. S., DeSilva, J. M., & Dominy, N. J. (2013a). Phenotypic plasticity of
979 climbing-related traits in the ankle joint of great apes and rainforest hunter-gatherers. *Human Biology*, 85,
980 309-328.

981 Venkataraman, V. V., Kraft, T. S., & Dominy, N. J. (2013b). Tree climbing and human evolution.
982 *Proceedings of the National Academy of Sciences*, 110, 1237-1242.

983 Vereecke, E., D'Août, K., De Clercq, D., Van Elsaker, L., & Aerts, P. (2003). Dynamic plantar pressure
984 distribution during terrestrial locomotion of bonobos (*Pan paniscus*). *American Journal of Physical*
985 *Anthropology*, 120, 373-383.

986 Wallace, I. J., Kwaczala, A. T., Judex, S., Demes, B., & Carlson, K. J. (2013). Physical activity
987 engendering loads from diverse directions augments the growing skeleton. *Journal of Musculoskeletal*
988 *and Neuronal Interactions*, 13, 283-288.

989 Wallace, I. J., Middleton, K. M., Lublinsky, S., Kelly, S. A., Judex, S., Garland, T., & Demes, B. (2010).
990 Functional significance of genetic variation underlying limb bone diaphyseal structure. *American Journal*
991 *of Physical Anthropology*, 143, 21-30.

992  Wan, L., de Asla, R. J., Rubash, H. E., & Li, G. (2006). Determination of *in-vivo* articular cartilage
993  contact areas of human talocrural joint under weightbearing conditions. *Osteoarthritis and Cartilage*, 14,
994  1294-1301.

995  Wang, W., Abboud, R. J., Günther, M. M., & Crompton, R. H. (2014). Analysis of joint force and torque
996  for the human and non-human ape foot during bipedal walking with implications for the evolution of the
997  foot. *Journal of Anatomy*, 225, 152-166.

998  Whitehouse, W. J. (1974). The quantitative morphology of anisotropic trabecular bone. *Journal of
999  Microscopy*, 101, 153-168.

1000 Wickham, H. (2009). *ggplot2: Elegant graphics for data analysis*. New York: Springer-Verlag.

1001 Worsley, K. J., Taylor, J. E., Carbonell, F., Chung, M. K., Duerden, E., Bernhardt, B., . . . Evans, A. C.
1002 (2009) SurfStat: A Matlab toolbox for the statistical analysis of univariate and multivariate surface and
1003 volumetric data using linear mixed effects models and random field theory. NeuroImage Organization for
1004 Human Brain Mapping Annual Meeting, 47, S102.

1005 Zeininger, A., Patel, B. A., Zipfel, B., Carlson, K. J. (2016). Trabecular architecture in the StW 352 fossil
1006 hominin calcaneus. *Journal of Human Evolution*, 97, 145-158.

1007 Zeininger, A., Richmond, B. G., & Hartman, G. (2011). Metacarpal head biomechanics: A comparative
1008 backscattered electron image analysis of trabecular bone mineral density in *Pan troglodytes*, *Pongo
1009 pygmaeus*, and *Homo sapiens*. *Journal of Human Evolution*, 60, 703-710.

1010 Zipfel, B., DeSilva, J. M., Kidd, R. S., Carlson, K. J., Churchill, S. E., & Berger, L. R. (2011). The foot
1011 and ankle of *Australopithecus sediba*. *Science*, 333, 1417-1420.

**Table 1. Study sample**

| Taxon | Body mass (kg)[3] | Locomotor behaviour | Tibia | Talus | Paired | Scan resolution (µm) | Relative resolution[4] |
|---|---|---|---|---|---|---|---|
| *Homo sapiens*[1] | 62.1-72.1 | Biped | 8 | 9 | 7 | 40 | 5.72-9.06 |
| *Pan troglodytes verus*[2] | 41.6-46.3 | Arboreal/knuckle-walker | 10 | 13 | 8 | 35 | 5.46-11.59 |

[1] Anthropological Collection of Institute of Zoology and Anthropology, University of Göttingen
[2] Max Planck Institute for Evolutionary Anthropology
[3] Sex specific mean body mass (F-M). Body masses from Smith and Jungers (1997)
[4] Relative resolution = mean trabecular thickness (mm)/resolution(mm)

**Table 2. Mean and standard deviation of trabecular and cortical parameters in the talus and distal tibia of *Homo* and *Pan*. Results of Mann-Whitney U test between taxa are shown, with significant differences in bold.**

| Element | Taxon | Tb.Th (mm) | BV.TV (%) | DA | BS/BV(mm$^{-1}$) | Cortical thickness (mm) |
|---------|-------|-----------|-----------|-----|---------|-------------------------|
| Talus | *Homo* | 0.26 (0.03) | 24.77 (2.17) | 0.14 (0.07) | 0.32 (0.05) | 0.45 (0.06) |
|  | *Pan* | 0.31 (0.04) | 34.65 (2.63) | 0.02 (0.02) | 0.19 (0.02) | 0.88 (0.19) |
|  | Significance | **<0.01** | **<0.01** | **<0.01** | **<0.01** | **<0.01** |
| Tibia | *Homo* | 0.25 (0.04) | 19.92 (2.87) | 0.29 (0.10) | 0.45 (0.08) | 0.63 (0.07) |
|  | *Pan* | 0.23 (0.02) | 24.17 (3.43) | 0.32 (0.06) | 0.31 (0.06) | 1.13 (0.19) |
|  | Significance | 0.17 | **0.02** | 0.51 | **<0.01** | **<0.01** |

**Table 3. Results of Spearman's correlation test to test relationship between trabecular parameters within *Homo* and *Pan* in the talus and distal tibia.**

| Element | Taxon | Parameter | Tb.Th | BV/TV | BS/BV | DA |
|---------|-------|-----------|-------|-------|-------|-----|
| Talus | *Homo* | BV/TV | 0.42 | - | | |
| | | BS/BV | -0.18 | **-0.92\*\*** | - | |
| | | DA | **-0.82\*\*** | -0.45 | 0.28 | - |
| | | CTh | 0.57 | 0.50 | -0.30 | **-0.72\*** |
| | *Pan* | BV/TV | **0.59\*** | - | | |
| | | BS/BV | -0.10 | **-0.80\*\*** | - | |
| | | DA | **-0.98\*\*** | **-0.66\*\*** | 0.16 | - |
| | | CTh | **0.84\*\*** | **0.63\*** | -0.24 | **-0.80\*\*** |
| Tibia | *Homo* | BV/TV | 0.71 | - | | |
| | | BS/BV | **-0.83\*\*** | **-0.90\*\*** | - | |
| | | DA | **-0.74\*** | -0.50 | 0.69 | - |
| | | CTh | 0.31 | 0.07 | -0.07 | -0.02 |
| | *Pan* | BV/TV | **0.75\*** | - | | |
| | | BS/BV | **-0.67\*** | **-0.95\*\*** | - | |
| | | DA | **-0.71\*** | -0.62 | 0.41 | - |
| | | CTh | **0.82\*\*** | **0.65\*** | **-0.66\*** | -0.44 |

P-values indicated as $p < 0.05$ * and $p < 0.01$ **

**Table 4. Results of principal component analyses showing percentage variance and loading for each principal component. The analysis was conducted separately for the talus and tibia, including Tb.Th, BV/TV, DA, BS/BV, and cortical thickness.**

| Element | Parameter | PC1 | PC2 | PC3 | PC4 | PC5 |
|---------|-----------|-----|-----|-----|-----|-----|
| Talus | % variance | 82.64 | 10.27 | 4.35 | 2.43 | 0.31 |
| | (cumulative) | (82.64) | (92.90) | (97.26) | (99.69) | (100.00) |
| | Tb.Th | **0.41** | **0.70** | 0.30 | **0.50** | -0.08 |
| | BV/TV | **0.48** | -0.28 | 0.09 | 0.08 | **0.82** |
| | DA | **-0.44** | -0.21 | **0.85** | 0.16 | 0.07 |
| | BS/BV | **-0.43** | **0.62** | -0.05 | **-0.40** | **0.51** |
| | Cortical thickness | **0.46** | 0.05 | **0.41** | **-0.75** | -0.22 |
| Tibia | % variance | 56.45 | 34.41 | 5.41 | 2.88 | 0.86 |
| | (cumulative) | (56.45) | (90.85) | (96.26) | (99.14) | (100.00) |
| | Tb.Th | 0.27 | **-0.65** | 0.03 | **-0.71** | -0.06 |
| | BV/TV | **0.57** | 0.13 | **0.42** | 0.06 | **0.69** |
| | DA | -0.30 | **0.62** | 0.29 | -0.67 | 0.02 |
| | BS/BV | **-0.55** | -0.22 | -0.36 | -0.09 | **0.72** |
| | Cortical thickness | **0.46** | 0.37 | **-0.78** | -0.20 | **0.**05 |

High loadings (i.e. greater than 0.40) are shown in bold

**Table 5. The relationship between bone structure and bone size in *Homo* and *Pan*. Results of OLS regression and Pearson's correlation for each trabecular parameter and cortical thickness against the geometric mean of several measurements, used as a proxy for bone size.**

| Taxon | Element | Parameter | Pearson's $r$ | Slope | Lower 95% CI | Upper 95% CI | $P$-value | $R^2$ |
|---|---|---|---|---|---|---|---|---|
| *Homo* | Talus | Tb.Th | -0.40 | -0.51 | -1.58 | 0.57 | 0.30 | 0.15 |
| | | BV/TV | -0.48 | -0.52 | -1.37 | 0.34 | 0.20 | 0.23 |
| | | DA | 0.10 | 2.01 | -4.28 | 8.29 | 0.48 | 0.08 |
| | | BS/BV | 0.33 | 0.59 | -1.23 | 2.41 | 0.47 | 0.08 |
| | | CTh | 0.12 | 0.23 | -1.23 | 1.70 | 0.72 | 0.02 |
| | Tibia | Tb.Th | 0.27 | 0.53 | -1.47 | 2.53 | 0.54 | 0.07 |
| | | BV/TV | 0.55 | 1.11 | -0.57 | 2.80 | 0.16 | 0.30 |
| | | DA | 0.09 | -0.05 | -6.71 | 6.61 | 0.99 | 0.00 |
| | | BS/BV | -0.51 | -1.35 | -3.56 | 0.87 | 0.19 | 0.27 |
| | | CTh | 0.25 | 0.38 | -1.19 | 1.95 | 0.57 | 0.06 |
| *Pan* | Talus | Tb.Th | 0.29 | 0.55 | -0.79 | 1.89 | 0.39 | 0.07 |
| | | BV/TV | -0.05 | -0.06 | -0.88 | 0.76 | 0.87 | 0.00 |
| | | DA | -0.11 | -2.97 | -11.57 | 5.62 | 0.46 | 0.05 |
| | | BS/BV | 0.12 | 0.25 | -1.15 | 1.65 | 0.70 | 0.01 |
| | | CTh | 0.19 | 0.60 | -1.55 | 2.75 | 0.55 | 0.03 |
| | Tibia | Tb.Th | 0.37 | 0.74 | -0.64 | 2.11 | 0.25 | 0.16 |
| | | BV/TV | 0.05 | 0.16 | -1.70 | 2.03 | 0.84 | 0.01 |
| | | DA | -0.35 | -1.22 | -3.98 | 1.54 | 0.34 | 0.11 |
| | | BS/BV | -0.04 | -0.04 | -3.36 | 3.27 | 0.98 | 0.00 |
| | | CTh | 0.28 | 0.80 | -1.32 | 2.93 | 0.41 | 0.09 |

**Table 6. Results of Pearson's correlation test to test relationship of each trabecular parameter and cortical thickness between the talus and distal tibia in *Homo* and *Pan*.**

| Taxa | Parameter | Pearson's *r* | *P*-value |
|---|---|---|---|
| *Homo* | Tb.Th | 0.83 | **0.02** |
| | BV/TV | 0.72 | 0.07 |
| | DA | 0.55 | 0.20 |
| | BS/BV | 0.83 | **0.02** |
| | Cortical thickness | 0.43 | 0.33 |
| *Pan* | Tb.Th | 0.86 | **0.01** |
| | BV/TV | 0.80 | **0.02** |
| | DA | 0.56 | 0.15 |
| | BS/BV | 0.81 | **0.02** |
| | Cortical thickness | 0.92 | **<0.01** |

Significant correlations are shown in bold ($p < 0.05$)

**Fig 1.** Processing steps for trabecular and cortical bone analysis for a *Pan* distal tibia. a) Segmented microCT scan. b) Segmented trabecular bone. c) Inner mask, where trabecular bone and internal region of the bone are assigned different grey values, and the cortical bone has been removed. A background grid and sampling sphere are applied to calculate trabecular structure throughout the bone. d) Tetrahedral mesh with colour scalars representing trabecular bone volume fraction. e) Unsegmented voxel data. f) Process of measurement of cortical thickness. g) Cortical thickness values mapped to a subject-specific surface. h) Each subject-specific surface (green) is registered to a canonical surface (red) for interspecific comparisons.
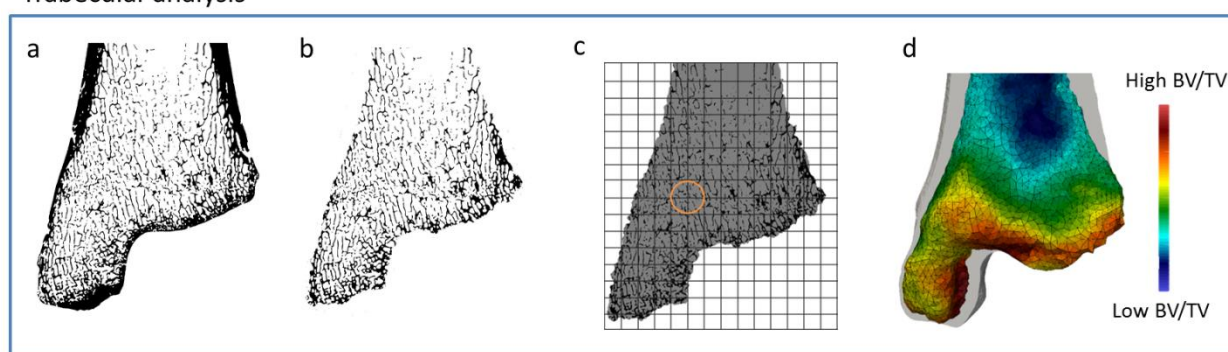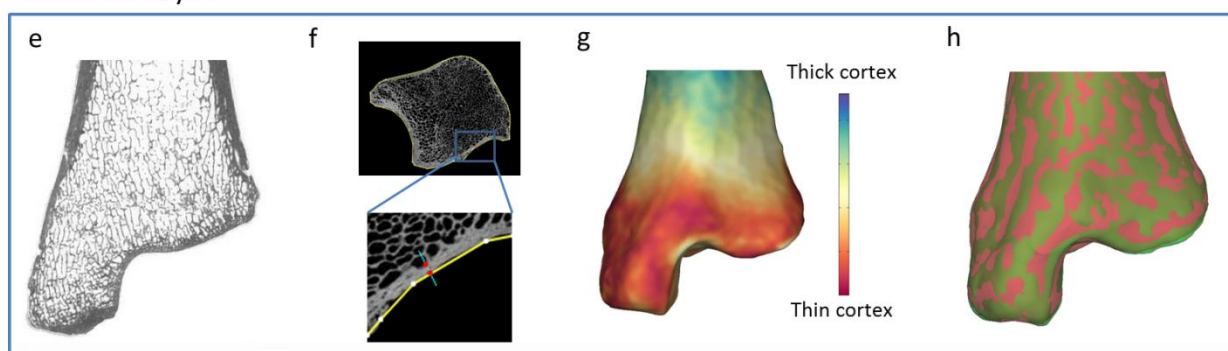
**Fig 2.** Extracted cubes of trabecular bone from approximately the same location in the talus and distal tibia of *Homo* and *Pan*.
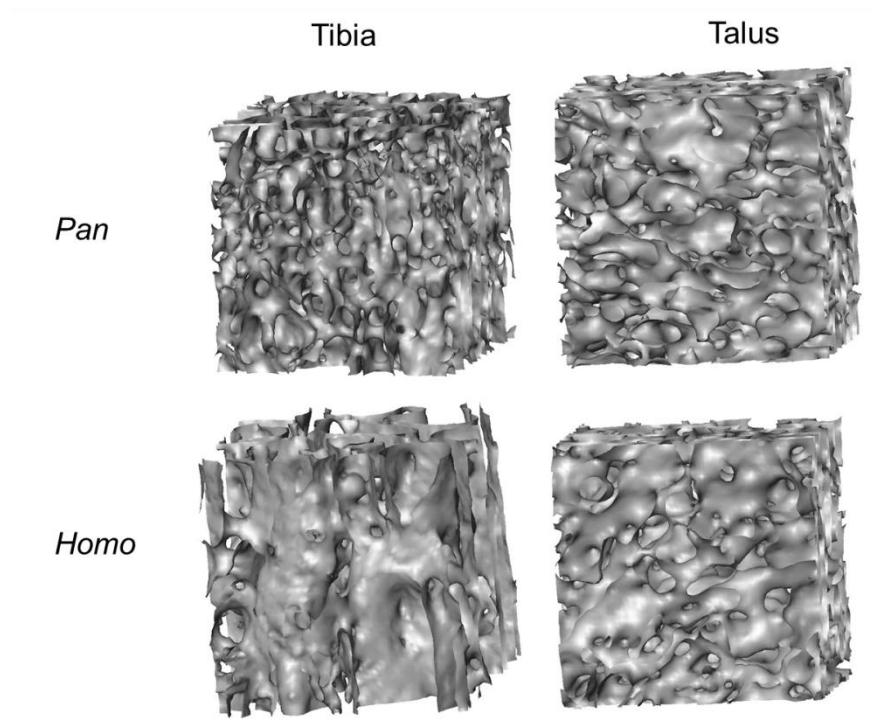
15   **Fig 3.** PC1 and PC2 for trabecular and cortical structure of the talus and distal tibia of *Pan* (blue)
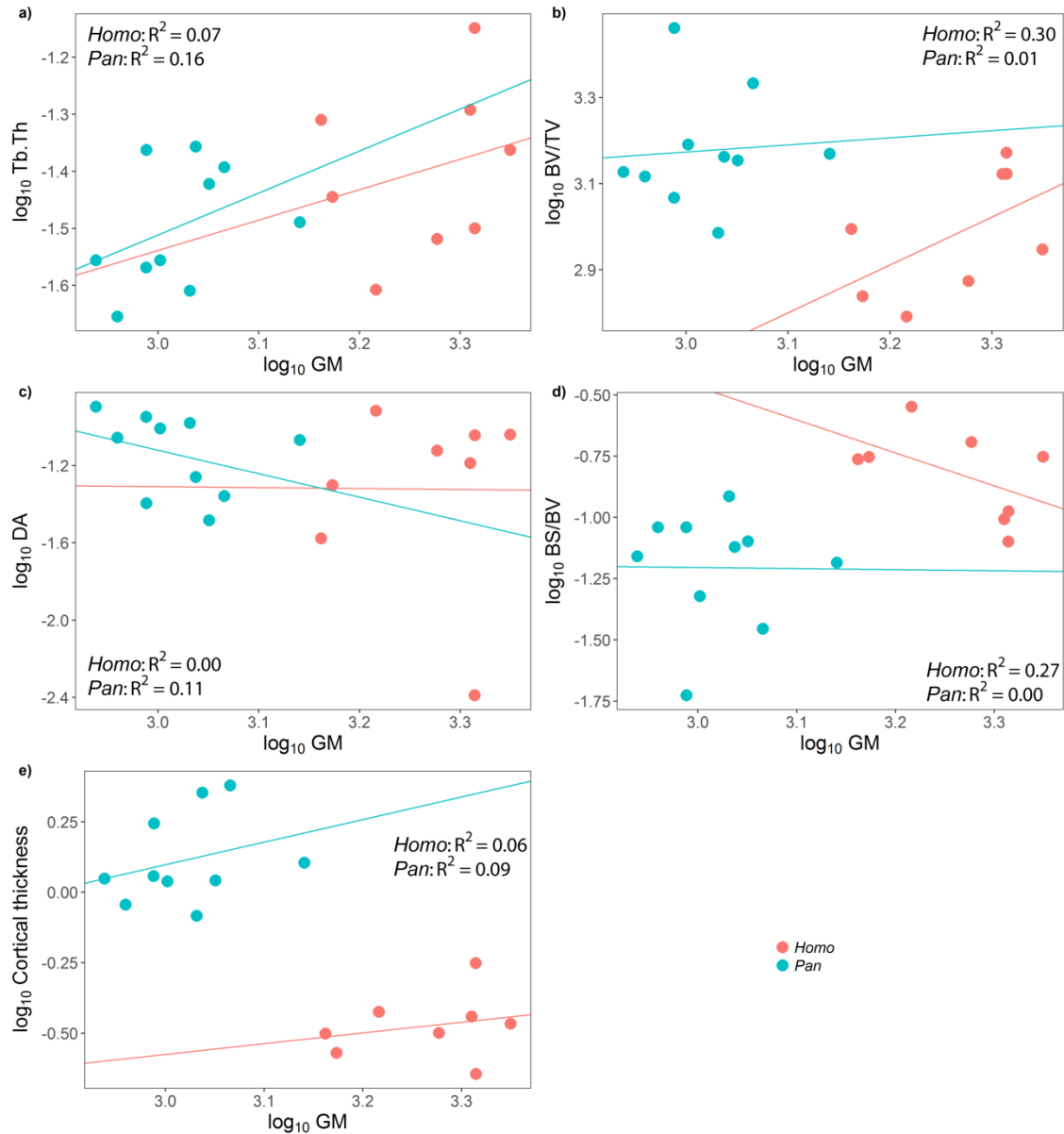
16   and *Homo* (red).
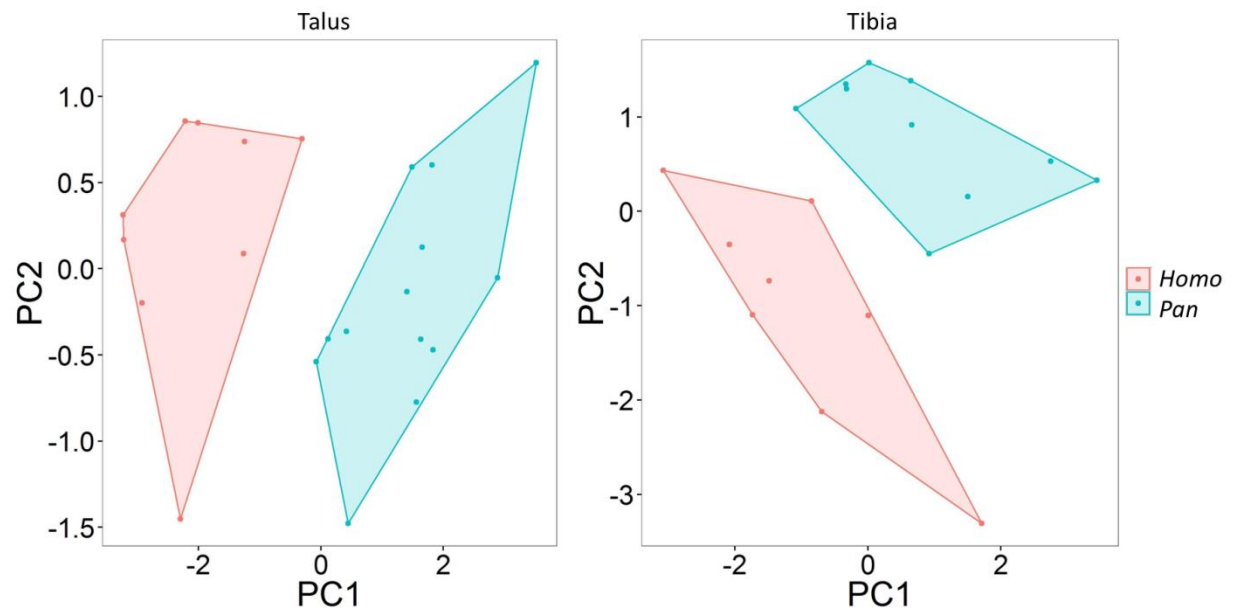


17

18

19    **Fig 4.** Relationship between talus size and trabecular and cortical parameters in *Pan* (blue) and

20    *Homo* (red). The $\log_{10}$ OLS regression lines are shown independently for *Pan* (blue) and *Homo*

21    (red).
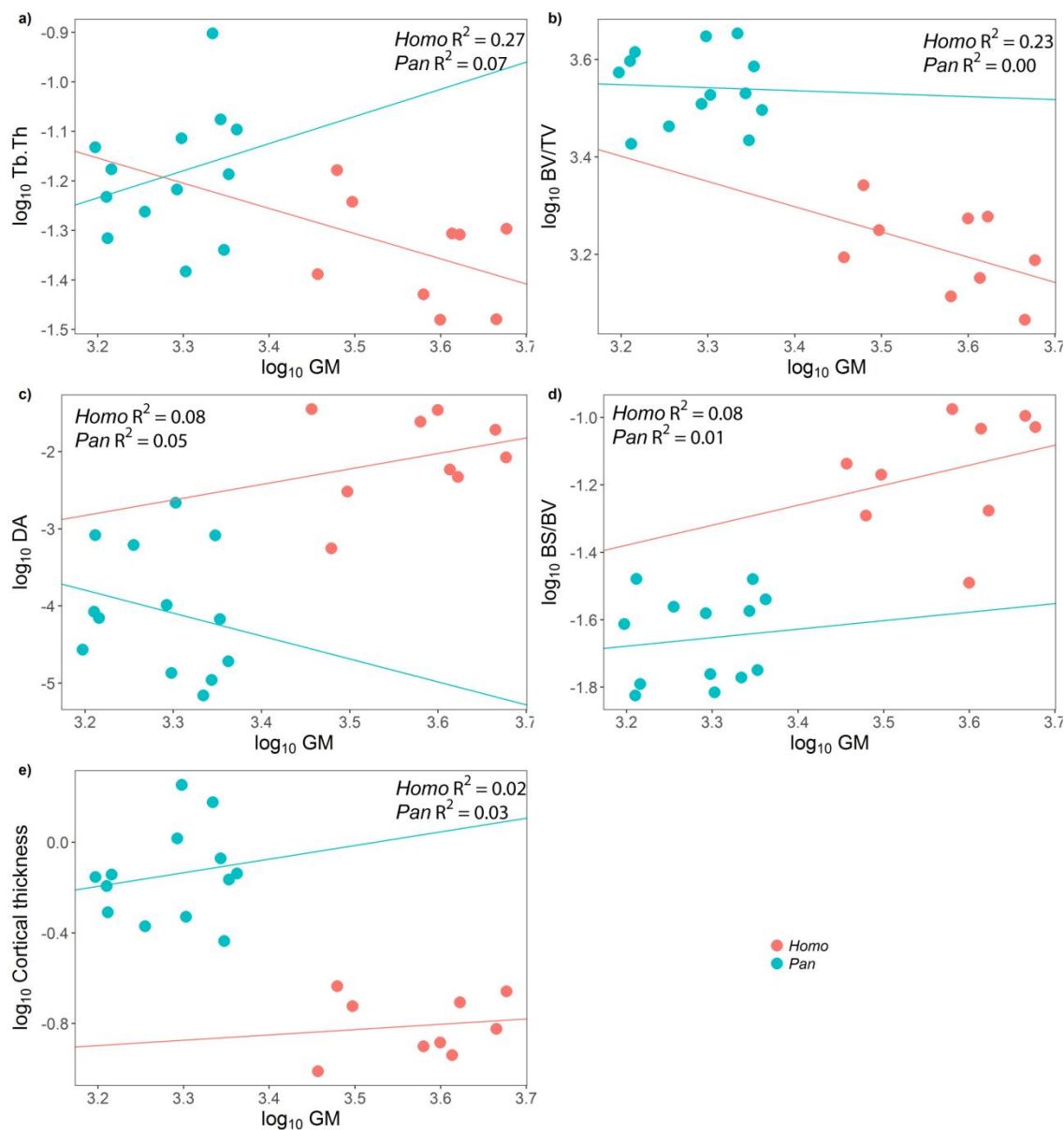


22

23

24 **Fig 5.** Relationship between tibia size and trabecular and cortical parameters in *Pan* (blue) and

25 *Homo* (red). The $\log_{10}$ OLS regression lines are shown independently for *Pan* (blue) and *Homo*

26 (red).



27

28

29   **Fig 6.** Comparison of trabecular and cortical structure between the talus and tibia in *Pan* (blue)

30   and *Homo* (red). The $\log_{10}$ RMA regression lines are shown independently for *Pan* (blue) and

31   *Homo* (red).



32

33
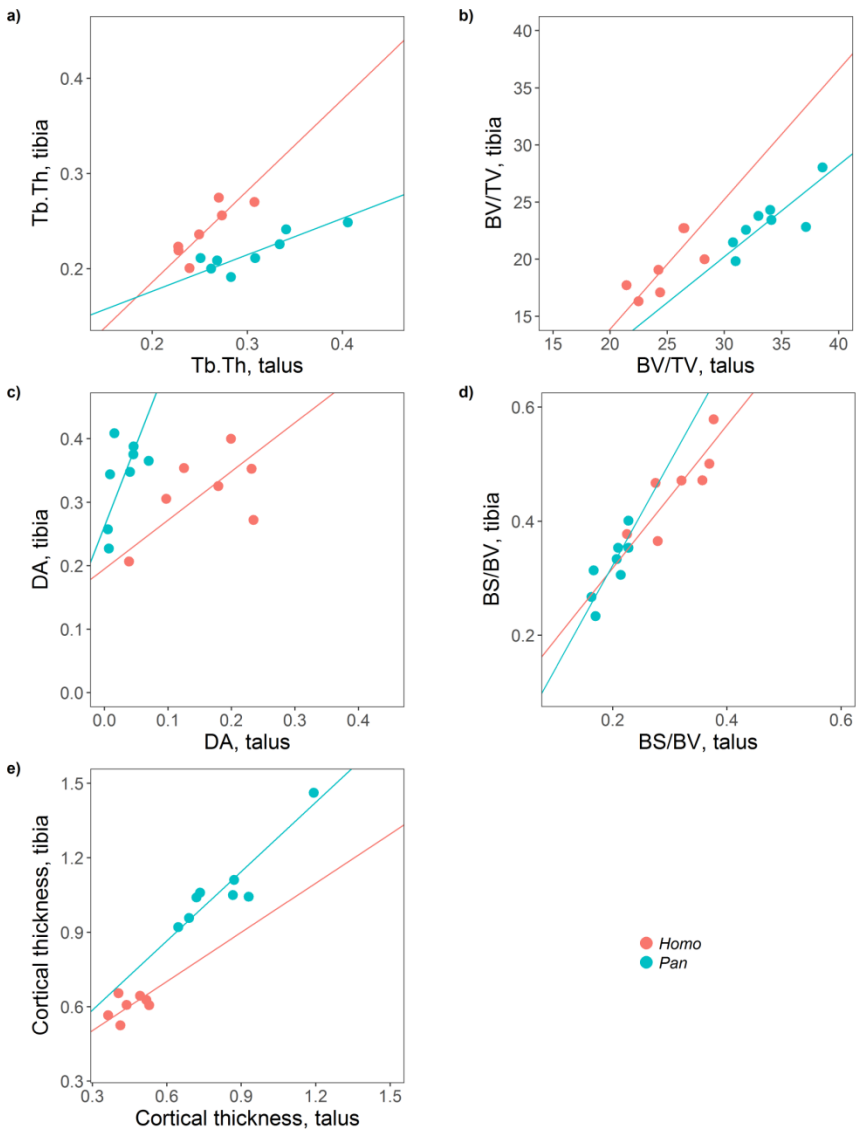
**Fig 7.** Morphometric maps of BV/TV in the talus  in one individual of *Homo* (a-e) and *Pan* (f-j) in (from top to bottom) dorsal view, mid-transverse plane, anterior view, coronal plane (in the centre of the trochlea), and sagittal plane (in the centre of the trochlea). Each specimen is scaled to its own data range, as shown in the scale bars. Black arrows indicate regions described in the text.
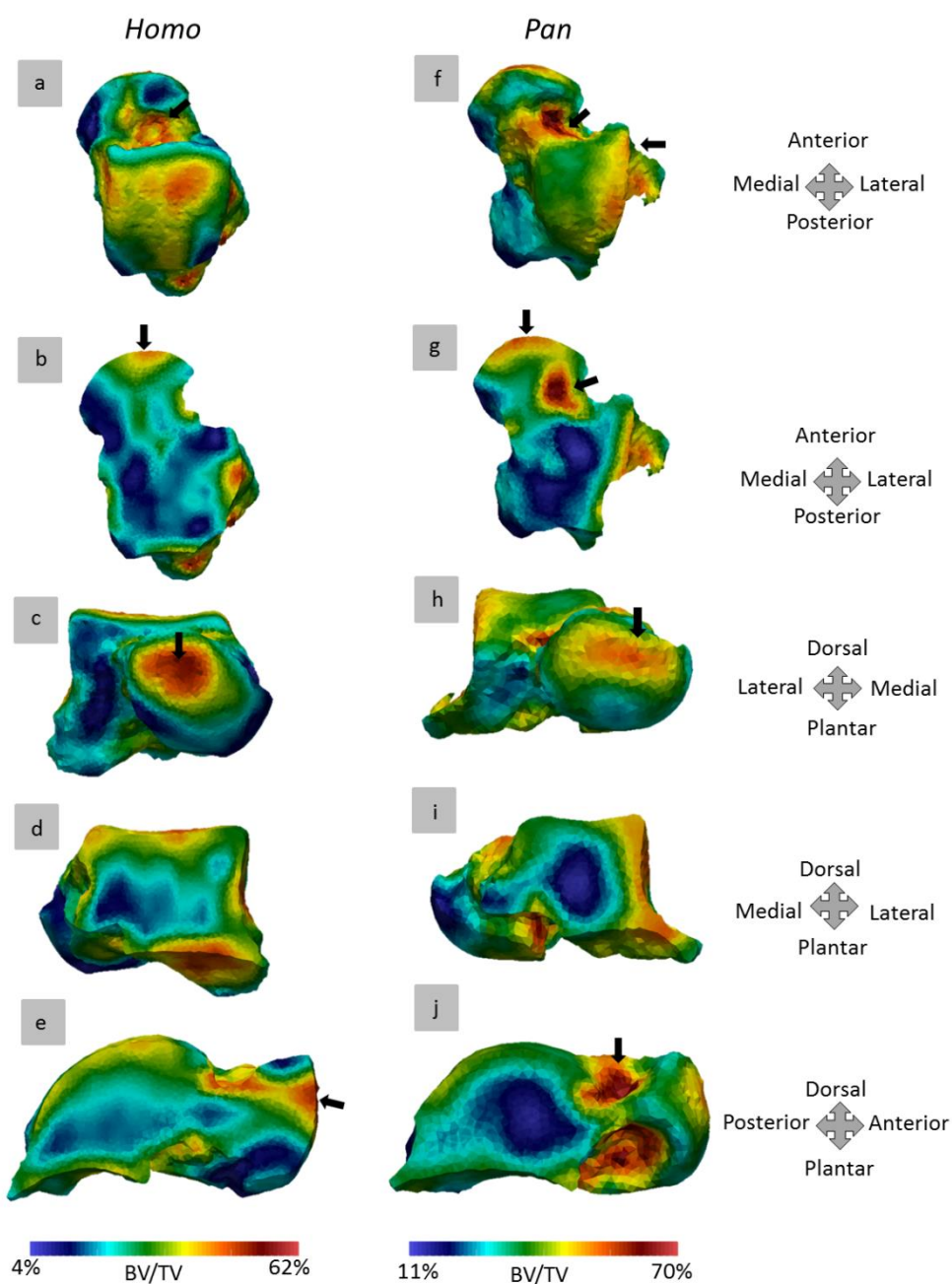
**Fig 8.** Morphometric maps of BV/TV in the tibia in one individual of *Homo* (a-e) and *Pan* (f-j) in (from top to bottom) distal view, mid-sagittal plane of distal tibia, anterior view and mid-coronal plane of distal tibia. Each specimen is scaled to its own data range, as shown in the scale bars. Black arrows indicate regions described in the text.
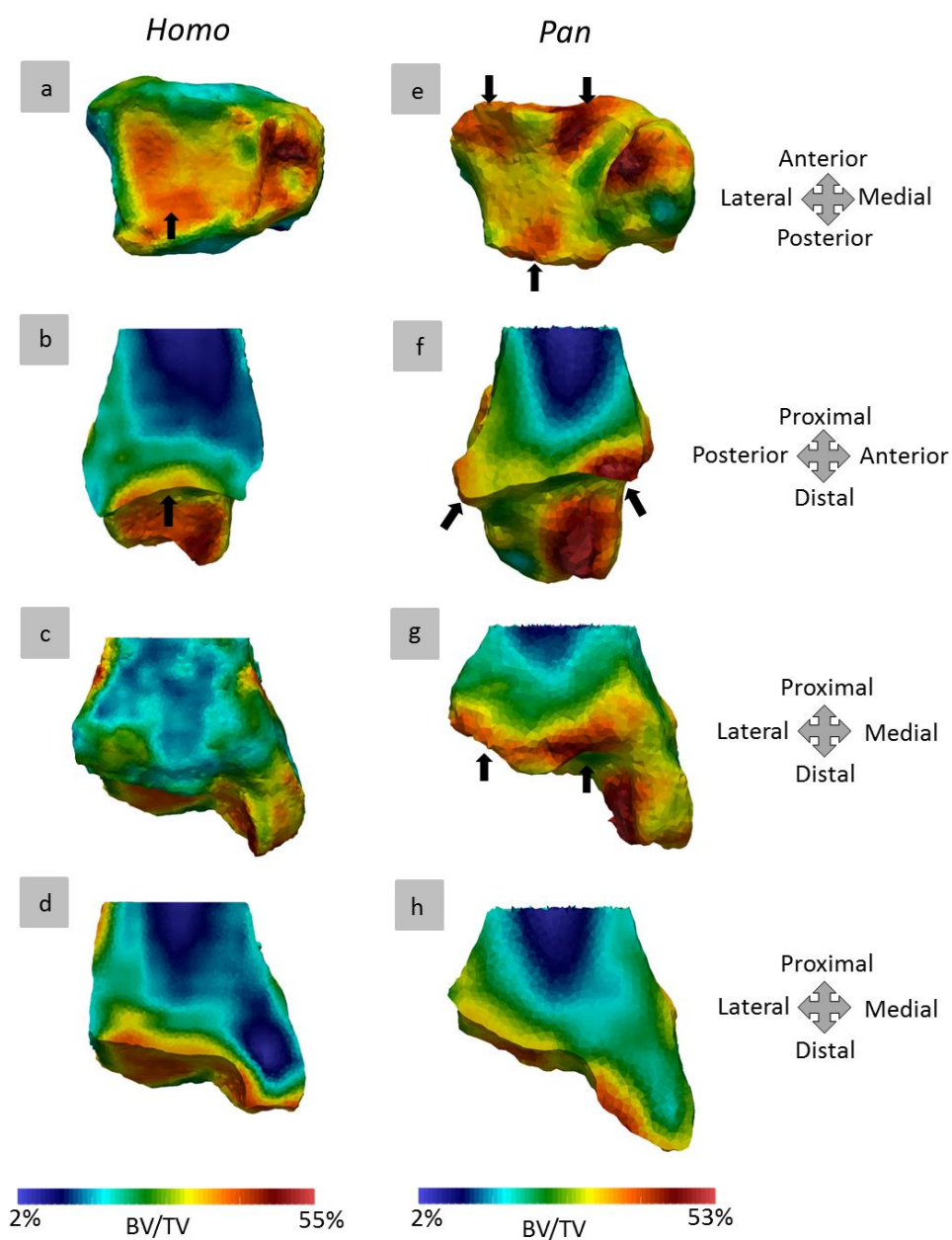
**Fig 9.** Morphometric maps of mean relative cortical thickness on the canonical talus in *Homo* (a) and *Pan* (b) in (from left to right) anterior, dorsal and plantar views. Red indicates thick regions and blue indicates thin regions. (c) Differences between the species are shown as the difference in *Pan* compared to *Homo* with positive values (red) indicating thicker bone and negative values (blue) indicating thinner bone. (d) Regions of significant differences between the species at vertices and clusters (red-yellow) and at clusters (blue) of the surface mesh.
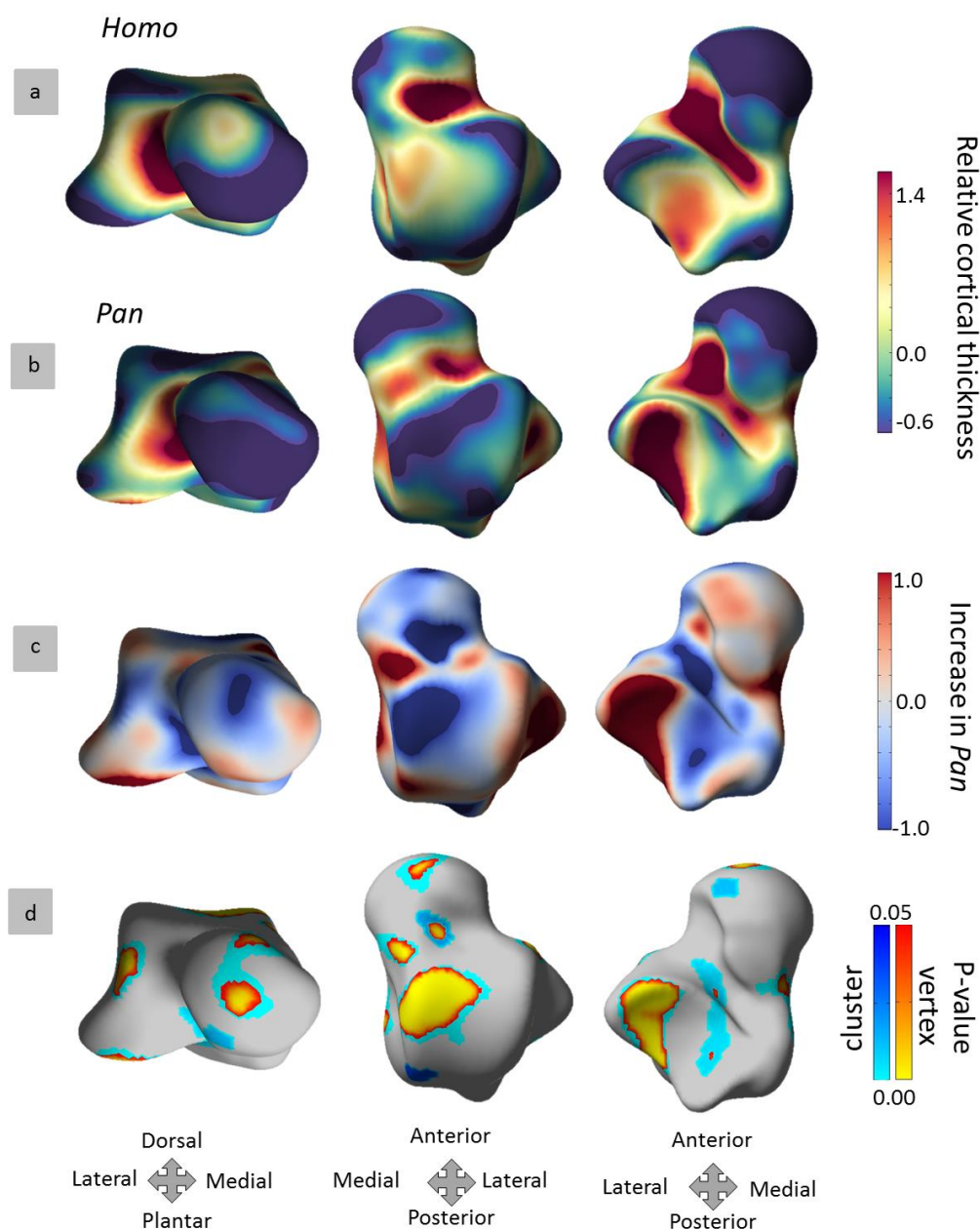
**Fig 10.** Morphometric maps of mean relative cortical thickness on the canonical tibia in (a) *Homo* and (b) *Pan* in (from left to right) lateral, distal and anterior views. Red indicates thick regions and blue indicates thin regions. (c) Differences between the species are shown as the difference in *Pan* compared to *Homo* with positive values (red) indicating thicker bone and negative values (blue) indicating thinner bone. (d) Regions of significant differences between the species at vertices and clusters (red-yellow) and at clusters (blue) of the surface mesh.